

AN *hp* MULTIGRID APPROACH FOR TENSOR-PRODUCT SPACE-TIME FINITE ELEMENT DISCRETIZATIONS OF THE STOKES EQUATIONS*

NILS MARGENBERG[†], MARKUS BAUSE[‡], AND PETER MUNCH[§]

Abstract. We present a monolithic *hp* space-time multigrid method for tensor-product space-time finite element discretizations of the Stokes equations. Geometric and polynomial coarsening of the space-time mesh is performed, and the entire algorithm is expressed through rigorous mathematical mappings. For the discretization, we use inf-sup stable pairs $\mathbb{Q}_{r+1}/\mathbb{P}_r^{\text{disc}}$ of elements in space and a discontinuous Galerkin (DG(k)) discretization in time with piecewise polynomials of order k . The key novelty of this work is the application of *hp* multigrid techniques in space and time, facilitated and accelerated by the matrix-free capabilities of the `deal.II` library. While multigrid methods are well-established for stationary problems, their application in space-time formulations encounter unique challenges, particularly in constructing suitable smoothers. To overcome these challenges, we employ a space-time cell-wise Vanka smoother. Extensive tests on high-performance computing platforms demonstrate the efficiency of our *hp* multigrid approach on problem sizes exceeding a trillion degrees of freedom (dofs), sustaining throughputs of hundreds of millions of dofs per second.

Key words. Space-time finite elements, space-time multigrid, monolithic multigrid, matrix-free, higher-order finite elements, high-performance computing

MSC codes. 65M60, 65M55, 65F10, 65Y05

1. Introduction. Time-dependent partial differential equations, such as the nonstationary Stokes equations, greatly benefit from methods that exploit parallelism in space and time. *Space-time finite element methods* (STFEMs) offer a natural framework for such parallelization by treating time as an additional dimension, enabling simultaneous discretization and solution in space and time.

In this work, we present a *hp* space-time multigrid method (*hp* STMG) for tensor-product space-time finite element discretizations of the Stokes system. For the discretization in space we use the mapped version of the inf-sup stable $\mathbb{Q}_{r+1}/\mathbb{P}_r^{\text{disc}}$ pairs of finite elements, with $r \in \mathbb{N}$. For the discretization in time, we use the discontinuous Galerkin method (DG(k)) of order $k \in \mathbb{N}$. Continuous in time Galerkin methods are not studied here, due to their difficulties related to the computation of a discrete initial value for the pressure and the non-wellposedness of the discrete pressure trajectory [6]. The key novelty of our approach is the application of geometric and polynomial space-time multigrid techniques. The implementation is facilitated by the matrix-free capabilities of the `deal.II` library [2, 28, 35, 17]. The present work builds upon the foundation established in [32]. The code is available on GitHub at <https://github.com/nlsmrg/dealii-stfem>.

Extending multigrid methods to STFEMs poses challenges, particularly in the design of effective smoothers for the arising linear systems. However, STFEMs offer appreciable advantages: They naturally integrate spatial and temporal discretizations and handle coupled problems. Further, they facilitate duality-based and goal-oriented adaptivity in space and time [8, 7, 42]. Adaptive STFEMs have also been investi-

*Submitted to the editors DATE.

[†]Helmut Schmidt University, Faculty of Mechanical and Civil Engineering, Holstenhofweg 85, 22043 Hamburg, Germany, margenbn@hsu-hh.de (Corresponding Author)

[‡]Helmut Schmidt University, Faculty of Mechanical and Civil Engineering, Holstenhofweg 85, 22043 Hamburg, Germany, bause@hsu-hh.de

[§]Technical University Berlin, Faculty of Mathematics, Straße des 17. Juni 136, 10623 Berlin, Germany, p.muench@tu-berlin.de

gated in [29, 49, 12]. Alternative approaches, particularly for unstructured space-time meshes are discussed in [31, 45, 36, 14, 30]. The utilization of global STFEMs, i.e. the concurrent treatment of all subintervals, has the potential to fully exploit the computational resources of high-performance computers. Conversely, local STFEMs employ space-time variational discretizations as time-marching schemes by selecting a test basis supported on the subintervals. This requires less computational resources, while scalability to global formulations is maintained. Finally, higher order FE spaces facilitate improved accuracy of discrete solutions on computationally feasible grids.

Parallel time integration methods have been developed to exploit parallelism in the time dimension and to overcome the sequential bottleneck of traditional time-stepping methods. A comprehensive review of such methods can be found in [19]. However, most of these methods entail a trade-off between additional computational complexity and time parallelism. An alternative is the all-at-once solution of the entire space-time system [13, 44]. Owing to the established connection between Runge–Kutta methods and variational time discretizations [20, 44], these contributions relate to the present work. Space-time multigrid methods treat time as an additional grid dimension, enabling simultaneous multilevel coarsening in space and time [24, 18, 16, 23]. While algebraic multigrid methods have been applied to space-time systems [46, 30], geometric multigrid techniques offer advantages in computational efficiency and scalability [22, 20]. Another approach to time parallelism that does not increase the computational complexity is stage parallelism within a single time step [11, 39, 34]. While the scalability of stage parallelism is constrained by the number of stages, these methods are effective in the scaling limit.

Our goal in this work is the design of a *hp* STMG with the same grid-independent convergence seen in established geometric multigrid techniques for elliptic or stationary Stokes-type problems [37]. For stability reasons, the *hp* STMG is applied as a preconditioner for GMRES iterations, which has become a standard approach in multigrid frameworks. For parallel efficiency, the *V*-cycle form is used, with a single *V*-cycle per application of *hp* STMG. The efficiency of multigrid methods strongly depend on the smoothing operator. We employ a space-time cell-wise Vanka smoother. Additive Schwarz or Vanka-type smoothers have a wide range of applications in fluid mechanics [3, 4], solid mechanics [50], fluid-structure interaction [15], dynamic poroelasticity [5] and acoustic wave equations [32]. To ensure computational efficiency of the *hp* STMG, we focus on the feasibility of matrix-free implementations.

In recent years, there has been work on matrix-free, high-order monolithic multigrid methods to solve Stokes (and Navier–Stokes) equations on high-performance computing architectures. The authors of [27] developed a parallel, matrix-free multigrid solver achieving “textbook multigrid efficiency”, scaling up to multiple trillions of unknowns. The authors of [1] extend a patch-based Vanka smoother to fully implicit Runge–Kutta discretizations of incompressible flows using standard Taylor–Hood elements. Jodlbauer et al. used a matrix-free monolithic geometric multigrid solver for discretizations of the Stokes equations with Taylor–Hood elements with scaled Chebyshev–Jacobi smoothers [25]. Prieto Saveedra et al. present a matrix-free solver for SUPG and PSPG stabilized equal-order discretizations of the incompressible Navier–Stokes equations, and achieve substantial speedups and reduced memory usage compared to matrix-based methods [41]. The authors of [48] propose a monolithic *ph*-multigrid method for stationary Stokes. In line with their findings, our experiments demonstrate that this approach outperforms geometric multigrid methods.

This paper is organized as follows. In Section 2 we introduce the continuous problem and the tensor-product space time finite element discretization. We formulate

the algebraic system arising from the discretization in Section 3. In Section 4 we introduce the hp STMG algorithm, which we use as a preconditioner to a GMRES method. We verify this methodology by numerical experiments in Section 5. We conclude with an evaluation of the results and a future outlook in Section 6.

2. Continuous and discrete problem.

2.1. Continuous problem. We consider the nonstationary Stokes system

$$\begin{aligned} (2.1a) \quad & \partial_t \mathbf{v} - \nu \Delta \mathbf{v} + \nabla p = \mathbf{f} \quad \text{in } \Omega \times (0, T), \\ (2.1b) \quad & \nabla \cdot \mathbf{v} = 0 \quad \text{in } \Omega \times (0, T), \\ (2.1c) \quad & \mathbf{v}(0) = \mathbf{v}_0 \quad \text{in } \Omega, \\ (2.1d) \quad & \mathbf{v} = \mathbf{0} \quad \text{on } \partial\Omega \times (0, T), \end{aligned}$$

where $\Omega \subset \mathbb{R}^d$, with $d \in \{2, 3\}$, is a bounded open Lipschitz domain and $T > 0$ is the final time. By \mathbf{v} and p we denote the unknown velocity and pressure field, respectively. The force \mathbf{f} and initial velocity \mathbf{v}_0 are prescribed data. In (2.1a), $\nu \in \mathbb{R}_{>0}$ denotes the fluid's viscosity. Homogeneous Dirichlet boundary conditions in (2.1d) are chosen for brevity of presentation. We assume that the Stokes system (2.1) admits a sufficiently regular solution up to $t = 0$ such that higher order approximations become feasible.

We use standard notation. $H^m(\Omega)$ is the Sobolev space of $L^2(\Omega)$ functions with derivatives up to order m in $L^2(\Omega)$ while $\langle \cdot, \cdot \rangle$ denotes the inner product in $L^2(\Omega)$ and its vector-valued and matrix-valued counterparts. Let $L_0^2(\Omega) := \{q \in L^2(\Omega) \mid \int_{\Omega} q \, dx = 0\}$ and $H_0^1(\Omega) := \{u \in H^1(\Omega) \mid u = 0 \text{ on } \partial\Omega\}$. We put $Q(\Omega) := L_0^2(\Omega)$ and $\mathbf{V}(\Omega) := H_0^1(\Omega)^d$. Here, bold-face letters are used to indicate vector-valued spaces and functions. Further, we define the space

$$\mathbf{V}^{\text{div}}(\Omega) := \{\mathbf{v} \in \mathbf{V} \mid \langle \nabla \cdot \mathbf{v}, q \rangle = 0 \ \forall q \in Q\}.$$

2.2. Space-time finite element discretization. For the discretization of (2.1) we use spatial and temporal finite element meshes, which are combined to a space-time mesh by an algebraic tensor-product. Discrete space-time function spaces are then defined in tensor-product form. For the time discretization, we partition the time interval $I := (0, T]$ into N equal subintervals $I_n := (t_{n-1}, t_n]$, for $n = 1, \dots, N$, where $t_n = n\tau$ and $\tau = T/N$. Thus, $I = \bigcup_{n=1}^N I_n$. The set $\mathcal{M}_\tau := \{I_1, \dots, I_N\}$ of time subintervals is called the time mesh. For any $k \in \mathbb{N}_0$ and Hilbert space H , we let $\mathbb{P}_k(J; H)$ denote the set of all polynomials of degree less than or equal to k on $J \subset I$ with values in H . Then, we put

$$Y_\tau^k(H) := \{w_\tau : I \rightarrow \mathbb{R} \mid w_\tau|_{I_n} \in \mathbb{P}_k(I_n; H) \ \forall I_n \in \mathcal{M}_\tau\}.$$

For spatial discretization, let \mathcal{T}_h be a shape-regular triangulation of Ω into quadrilateral and hexahedral elements in two and three space dimensions with mesh size $h > 0$. These element types are chosen for our implementation that is based on the deal.II library [2]. By $\mathbf{V}_{r+1}(K)$ and $Q_r(K)$ we denote the vector- and scalar-valued spaces on K of mapped polynomials from $(\mathbb{Q}_{r+1})^d$ and $\mathbb{P}_r^{\text{disc}}$, respectively, for some $r \geq 1$; cf. [26, Subsection 3.64]. The mapping are defined by the multilinear reference transformation of polynomials on the reference element. The finite element spaces to

be used for approximating \mathbf{V} and Q and defining the hp STMG are

$$(2.2a) \quad \mathbf{V}_h^{r+1}(\Omega) := \{\mathbf{v}_h \in \mathbf{V} : \mathbf{v}_{h|K} \in \mathbf{V}_{r+1}(K) \text{ for all } K \in \mathcal{T}_h\} \cap \mathbf{H}_0^1(\Omega),$$

$$(2.2b) \quad Q_h^r(\Omega) := \{q_h \in Q : q_{h|K} \in Q_r(K) \text{ for all } K \in \mathcal{T}_h\},$$

$$(2.2c) \quad Q_h^{r,+}(\Omega) := Q_h^r(\Omega) \oplus \text{span}\{1\}.$$

The definition of Q_h^r leads to a discontinuous (in space) pressure approximation. Further, $Q_h^{r,+}(\Omega)$ is the pressure finite element space without orthogonality condition. The space of discretely divergence-free functions is given by

$$(2.3) \quad \mathbf{V}_h^{\text{div}}(\Omega) := \{\mathbf{v}_h \in \mathbf{V}_h^r \mid \langle \nabla \cdot \mathbf{v}_h, q_h \rangle = 0 \text{ for all } q_h \in Q_h\}.$$

The global discrete solution spaces are defined by the tensor-products

$$(2.4) \quad \mathbf{H}_{\tau,h}^v = Y_\tau^k(I) \otimes \mathbf{V}_h^{r+1}(\Omega), \quad H_{\tau,h}^p = Y_\tau^k(I) \otimes Q_h^r(\Omega).$$

Remark 2.1 (Function spaces and their tensor product structure).

- The algebraic tensor product $Y_\tau(I) \otimes V_h(\Omega)$ of two finite element spaces $Y_\tau(I)$ and $V_h(\Omega)$ is defined by

$$Y_\tau(I) \otimes V_h(\Omega) := \text{span}\{f \otimes g \mid f \in Y_\tau(I), g \in V_h(\Omega)\},$$

with mapping $f \otimes g : (t, \mathbf{x}) \rightarrow f(t)g(\mathbf{x})$. For the construction principle of tensor products of Hilbert spaces we refer to, e.g., [40, Subsection 1.2.3].

- The spaces $Y_\tau^k(I; \mathbf{V}_h^{r+1}(\Omega))$ and $Y_\tau^k(I; Q_h^r(\Omega))$ are isometric to the Hilbert spaces $\mathbf{H}_{\tau,h}^v$ and $H_{\tau,h}^p$, respectively; cf. [40, Proposition 1.2.28].

For any function $w : I \rightarrow \mathbf{V}_h$ that is piecewise sufficiently smooth with respect to the time mesh \mathcal{M}_τ , for instance for $w \in \mathbf{H}_{\tau,h}^v$, we define the right-hand side limit at a point t_n by $w^+(t_n) := \lim_{t \rightarrow t_n+0} w(t)$ for $0 < n < N$. Now, we introduce the fully discrete space-time finite element approximation of (2.1).

Problem 2.2 (Discrete variational problem). Let the data $\mathbf{f} \in L^2(I; L^2(\Omega))$ and an approximation $\mathbf{v}_{0,h} \in V_h^{\text{div}}(\Omega)$ of $\mathbf{v}_0 \in \mathbf{V}^{\text{div}}(\Omega)$ be given. Put $\mathbf{v}_{\tau,h}(t_0) := \mathbf{v}_{0,h}$. Find $(\mathbf{v}_{\tau,h}, p_{\tau,h}) \in \mathbf{H}_{\tau,h}^v \times H_{\tau,h}^p$ such that for all $n = 1, \dots, N$ and $(\mathbf{w}_{\tau,h}, q_{\tau,h}) \in \mathbf{H}_{\tau,h}^v \times H_{\tau,h}^p$ there holds that

$$(2.5a) \quad \sum_{n=1}^N \int_{t_{n-1}}^{t_n} \langle \partial_t \mathbf{v}_{\tau,h}, \mathbf{w}_{\tau,h} \rangle + \nu \langle \nabla \mathbf{v}_{\tau,h}, \nabla \mathbf{w}_{\tau,h} \rangle - \langle p_{\tau,h}, \nabla \cdot \mathbf{w}_{\tau,h} \rangle dt \\ + \sum_{n=0}^{n-1} \langle \llbracket \mathbf{v}_{\tau,h} \rrbracket_n, \mathbf{w}_{\tau,h}^+(t_n) \rangle = \sum_{n=1}^N \int_{t_{n-1}}^{t_n} \langle \mathbf{f}, \mathbf{w}_{\tau,h} \rangle dt,$$

$$(2.5b) \quad \sum_{n=1}^N \int_{t_{n-1}}^{t_n} \langle \nabla \cdot \mathbf{v}_{\tau,h}, q_{\tau,h} \rangle dt = 0,$$

with the jump $\llbracket \mathbf{v}_{\tau,h} \rrbracket_n := \mathbf{v}_{\tau,h}^+(t_n) - \mathbf{v}_{\tau,h}(t_n)$.

Well-posedness of Problem 2.2 can be shown along the lines of [5, Lemma 3.2].

3. Algebraic system. Here, we rewrite Problem 2.2 in its algebraic form by exploiting the tensor product structure (2.4) of the discrete spaces. In Section 4 we then embed the algebraic system into an hp multigrid approach.

3.1. Preliminaries. For time integration in (2.5), it is natural to apply the right-sided $(k+1)$ -point Gauss–Radau quadrature formula. On I_n , it reads as

$$(3.1) \quad Q_n(w) := \frac{\tau_n}{2} \sum_{\mu=1}^{k+1} \hat{\omega}_\mu w(t_n^\mu) \approx \int_{I_n} w(t) dt,$$

where $t_n^\mu = T_n(\hat{t}_\mu)$, for $\mu = 1, \dots, k+1$, are the Gauss–Radau quadrature points on I_n and $\hat{\omega}_\mu$ the corresponding weights. Here, $T_n(\hat{t}) := (t_{n-1} + t_n)/2 + (\tau_n/2)\hat{t}$ is the affine transformation from $\hat{I} = [-1, 1]$ to I_n and \hat{t}_μ are the Gauss–Radau quadrature points on \hat{I} . The quadrature rule (3.1) is exact for all $w \in \mathbb{P}_{2k}(I_n; \mathbb{R})$, and $t_n^{k+1} = t_n$.

For time interpolation, a Lagrangian basis with respect to the Gauss–Radau quadrature points and with local support on the subintervals I_n , for $n = 1, \dots, N$, is used,

$$(3.2) \quad \begin{aligned} Y_\tau^k(I) = \text{span} \{ & \varphi_n^a \in L^2(I) \mid \varphi_n^a|_{I_b} \in \mathbb{P}_k(I_b; \mathbb{R}), \text{ for } b = 1, \dots, N, \\ & \text{supp } \varphi_n^a \subset \bar{I}_n, \varphi_n^a(t_n^\mu) = \delta_{a,\mu}, \text{ for } \mu = 1, \dots, k+1, \\ & \text{and for } a = 1, \dots, k+1, n = 1, \dots, N \}, \end{aligned}$$

with the Kronecker symbol $\delta_{a,\mu}$. For space discretization, we use the standard (global) finite element bases associated with the spaces (2.2) and put

$$(3.3a) \quad \mathbf{V}_h^{r+1}(\Omega) = \text{span} \{ \chi_m^v \mid m = 1, \dots, M^v \}$$

$$(3.3b) \quad Q_h^{r,+}(\Omega) = \text{span} \{ \chi_m^p \mid m = 1, \dots, M^p \}.$$

Then, functions $(\mathbf{v}_{\tau,h}, p_{\tau,h}) \in \mathbf{H}_{\tau,h}^v \times H_{\tau,h}^p$ admit for $\mathbf{x} \in \Omega$ and $t \in I$ the representation

$$(3.4a) \quad \mathbf{v}_{\tau,h}(\mathbf{x}, t) = \sum_{n=1}^N \sum_{a=1}^{k+1} \sum_{m=1}^{M^v} v_n^{a,m} \varphi_n^a(t) \chi_m^v(\mathbf{x}),$$

$$(3.4b) \quad p_{\tau,h}(\mathbf{x}, t) = \sum_{n=1}^N \sum_{a=1}^{k+1} \sum_{m=1}^{M^p} p_n^{a,m} \varphi_n^a(t) \chi_m^p(\mathbf{x})$$

with coefficients $v_n^{a,m} \in \mathbb{R}^d$ and $p_n^{a,m} \in \mathbb{R}$ for $n = 1, \dots, N$, $a = 1, \dots, k+1$ and $m = 1, \dots, M$, with $M \in \{M^v, M^p\}$. This representation again shows the tensor-product structure, which we exploit here. We note that the orthogonality condition for the pressure is not implemented yet in (3.4b), this will be done below in the multigrid framework in Subsection 4.1.

To recast (2.5) in algebraic form, we use a local (i.e., on each subinterval I_n) space and variable major order of the coefficients $v_n^{a,m} \in \mathbb{R}$ and $p_n^{a,m} \in \mathbb{R}$. For this, we introduce the column vectors

$$(3.5) \quad \mathbf{V}_n^a := (v_n^{a,1}, \dots, v_n^{a,M^v})^\top \in \mathbb{R}^{M^v}, \quad \mathbf{P}_n^a := (p_n^{a,1}, \dots, p_n^{a,M^p})^\top \in \mathbb{R}^{M^p},$$

for $a = 1, \dots, k+1$. From (3.5) we define the column vectors

$$(3.6) \quad \mathbf{V}_n := (\mathbf{V}_n^1, \dots, \mathbf{V}_n^{k+1})^\top \in \mathbb{R}^{(k+1) \cdot M^v}, \quad \mathbf{P}_n := (\mathbf{P}_n^1, \dots, \mathbf{P}_n^{k+1})^\top \in \mathbb{R}^{(k+1) \cdot M^p}$$

for $n = 1, \dots, N$. For improved readability, the transpose sign is skipped for the subvectors \mathbf{V}_n^a and \mathbf{P}_n^a in (3.6). Throughout the paper, we don't differ in the notation between column and row vectors, if the meaning is clear from the context. The global

column vector \mathbf{X} of unknowns on $\Omega \times I$, with $\mathbf{X}_n = (\mathbf{V}_n, \mathbf{P}_n)^\top \in \mathbb{R}^{(k+1) \cdot (M^v + M^p)}$ for $n = 1, \dots, N$, is then defined by

$$(3.7) \quad \mathbf{X} = (\mathbf{X}_1, \dots, \mathbf{X}_N)^\top := (\mathbf{V}_1, \mathbf{P}_1, \dots, \mathbf{V}_N, \mathbf{P}_N)^\top \in \mathbb{R}^{N \cdot (k+1) \cdot (M^v + M^p)}.$$

For the temporal finite element basis induced by (3.2), we define the local matrices $\mathbf{K}_n^\tau \in \mathbb{R}^{(k+1), (k+1)}$, $\mathbf{M}_n^\tau \in \mathbb{R}^{(k+1), (k+1)}$ and $\mathbf{C}_n^\tau \in \mathbb{R}^{(k+1), (k+1)}$ by

$$(3.8a) \quad (\mathbf{K}_n^\tau)_{a,b} := \int_{t_{n-1}}^{t_n} \partial_t \varphi_n^b(t) \varphi_n^a(t) dt + \varphi_n^b(t_{n-1}^+) \varphi_n^a(t_{n-1}^-),$$

$$(3.8b) \quad (\mathbf{M}_n^\tau)_{a,b} := \int_{t_{n-1}}^{t_n} \varphi_n^b(t) \varphi_n^a(t) dt,$$

$$(3.8c) \quad (\mathbf{C}_n^\tau)_{a,b} := \begin{cases} \varphi_{n-1}^b(t_{n-1}) \varphi_n^a(t_{n-1}^+), & \text{for } n > 1, \\ \varphi_n^a(t_{n-1}^+), & \text{for } b = k+1, \\ 0, & \text{for } b \in \{1, \dots, k\}, \end{cases} \quad \text{for } n=1,$$

for $a, b = 1, \dots, k+1$. For the spatial finite element basis induced by (3.3), we let $\mathbf{M}_h^v \in \mathbb{R}^{M^v, M^v}$, $\mathbf{A}_h \in \mathbb{R}^{M^v, M^v}$, $\mathbf{B} \in \mathbb{R}^{M^p, M^p}$ and $\mathbf{M}_h^p \in \mathbb{R}^{M^p, M^p}$ be defined by

$$(3.9a) \quad (\mathbf{M}_h)_{i,j} := \int_{\Omega} \chi_j^v(\mathbf{x}) \chi_i^v(\mathbf{x}) d\mathbf{x}, \quad (\mathbf{A}_h)_{i,j} := \int_{\Omega} \nabla \chi_j^v(\mathbf{x}) \cdot \nabla \chi_i^v(\mathbf{x}) d\mathbf{x},$$

$$(3.9b) \quad (\mathbf{B}_h)_{l,j} := \int_{\Omega} \nabla \cdot \chi_j^v(\mathbf{x}) \chi_l^p(\mathbf{x}) d\mathbf{x}, \quad (\mathbf{M}_h^p)_{l,m} := \int_{\Omega} \chi_m^p(\mathbf{x}) \chi_l^p(\mathbf{x}) d\mathbf{x}$$

for $i, j = 1, \dots, M^v$ and $l, m = 1, \dots, M^p$. Next, we introduce the right-hand side column vector

$$(3.10) \quad \mathbf{B} = (\mathbf{B}_1, \dots, \mathbf{B}_N)^\top \in \mathbb{R}^{N \cdot (k+1) \cdot (M^v + M^p)}, \quad \text{with } \mathbf{B}_n = (\mathbf{F}_n, \mathbf{0})^\top$$

for $n = 1, \dots, N$ and subvectors \mathbf{F}_n defined by

$$(3.11) \quad \mathbf{F}_n := (\mathbf{F}_n^1, \dots, \mathbf{F}_n^{k+1})^\top \in \mathbb{R}^{(k+1) \times M^v}, \quad \text{with } (\mathbf{F}_n^a)_i := Q_n(\langle \mathbf{f}, \varphi_n^a \chi_i^v \rangle)$$

for $a = 1, \dots, k+1$ and $i = 1, \dots, M^v$, and with the quadrature formula (3.1). For the well-definedness of $(\mathbf{F}_n^a)_i$ in (3.11) we tacitly make the stronger regularity assumption that $\mathbf{f} \in C(I; \mathbf{L}^2(\Omega))$ is satisfied.

Finally, we recall the tensor (or right Kronecker) product $\mathbf{A} \otimes \mathbf{B}$ of matrices $\mathbf{A} \in \mathbb{R}^{r,r}$ and $\mathbf{B} \in \mathbb{R}^{s,s}$, for $r, s \in \mathbb{N}$, defined by

$$(3.12) \quad \mathbf{A} \otimes \mathbf{B} := \begin{pmatrix} a_{1,1} \mathbf{B} & \cdots & a_{1,r} \mathbf{B} \\ \vdots & \ddots & \vdots \\ a_{r,1} \mathbf{B} & \cdots & a_{r,r} \mathbf{B} \end{pmatrix} = (a_{ij} \mathbf{B})_{i,j=1}^r.$$

3.2. Algebraic form of the discrete problem. In Problem 2.2 we choose a tensor product basis of the solution and test space, with the natural Lagrangian basis of (3.2) built of functions supported on a single subinterval I_n . Then we recast for (2.5) the following sequence of local problems on I_n .

Problem 3.1 (Local algebraic problem). Let $n \in \{1, \dots, N\}$. For $n > 1$ let $\mathbf{v}_{\tau,h}(t_{n-1}) = \sum_{m=1}^{M^v} v_{n-1}^{k+1,m} \chi_m^v$. For $n = 1$ and $\mathbf{v}_{0,h} \in \mathbf{V}_h^{\text{div}}$ let $\mathbf{v}_{0,h} = \sum_{m=1}^{M^v} v_0^m \chi_m^v$. Put

$$(3.13) \quad \mathbf{V}_{n-1} := \begin{cases} (\mathbf{0}, \dots, \mathbf{0}, v_{n-1}^{k+1,1}, \dots, v_{n-1}^{k+1,M^v})^\top, & \text{for } n > 1, \\ (\mathbf{0}, \dots, \mathbf{0}, v_0^1, \dots, v_0^{M^v})^\top, & \text{for } n = 1. \end{cases}$$

Find $(\mathbf{V}_n, \mathbf{P}_n) \in \mathbb{R}^{(k+1)(M^v+M^p)}$ such that

$$(3.14) \quad \begin{pmatrix} \mathbf{K}_n^\tau \otimes \mathbf{M}_h + \mathbf{M}_n^\tau \otimes \mathbf{A}_h & \mathbf{M}_n^\tau \otimes \mathbf{B}_h^\top \\ \mathbf{M}_n^\tau \otimes \mathbf{B}_h & \mathbf{0} \end{pmatrix} \begin{pmatrix} \mathbf{V}_n \\ \mathbf{P}_n \end{pmatrix} = \begin{pmatrix} \mathbf{F}_n \\ \mathbf{0} \end{pmatrix} + \mathbf{C}_n^\tau \otimes \begin{pmatrix} \mathbf{M}_h \\ \mathbf{0} \end{pmatrix} \mathbf{V}_{n-1}.$$

We note that the orthogonality condition for the pressure has not been implemented yet in Problem 3.1. This will be done in the multigrid method by applying the occurring operators to a subspace of $\mathbf{R}^{(k+1) \cdot M^p}$, introduced in (4.6) below. For (3.14) along with (3.8) and (3.9) we introduce the abbreviations

$$(3.15) \quad \mathbf{D}_{\tau,h}^n := \begin{pmatrix} \mathbf{K}_n^\tau \otimes \mathbf{M}_h + \mathbf{M}_n^\tau \otimes \mathbf{A}_h & \mathbf{M}_n^\tau \otimes \mathbf{B}_h^\top \\ \mathbf{M}_n^\tau \otimes \mathbf{B}_h & \mathbf{0} \end{pmatrix}, \quad \mathbf{C}_{\tau,h}^n := -\mathbf{C}_n^\tau \otimes \begin{pmatrix} \mathbf{M}_h \\ \mathbf{0} \end{pmatrix}.$$

From the local system (3.14) on I_n we then get the following global problem on I .

Problem 3.2 (Global algebraic problem). Let \mathbf{V}_0 be defined by (3.13). Find $\mathbf{X} = (\mathbf{X}_1, \dots, \mathbf{X}_N) \in \mathbb{R}^{N \cdot (k+1) \cdot (M^v+M^p)}$ such that

$$(3.16) \quad \begin{pmatrix} \mathbf{D}_{\tau,h}^1 & & & & \\ \mathbf{C}_{\tau,h}^2 & \mathbf{D}_{\tau,h}^2 & & & \\ & & \ddots & & \\ & & & \ddots & \\ & & & & \mathbf{C}_{\tau,h}^N & \mathbf{D}_{\tau,h}^N \end{pmatrix} \begin{pmatrix} \mathbf{X}_1 \\ \vdots \\ \vdots \\ \vdots \\ \mathbf{X}_N \end{pmatrix} = \begin{pmatrix} \mathbf{B}_1 - \mathbf{C}_{\tau,h}^1 \mathbf{V}_0 \\ \vdots \\ \vdots \\ \mathbf{B}_N \end{pmatrix}.$$

The subvectors and -matrices in (3.16) are defined by (3.15) along with (3.8) to (3.11).

Remark 3.3 (Global linear system of Problem 3.2).

- Our hp STMG employs the global system representation (3.16). The formulation, that orders the unknowns by time and local variables as defined in (3.7), offers the appreciable advantage of allowing for the restriction of the temporal multigrid to a smaller number $\tilde{N} < N$ of subintervals by combining \tilde{N} subintervals to a macro time step. Thereby, the approach can be adapted to the available computer hardware in a flexible manner. Conversely, solving the entire system (3.16) for a high number of subintervals demands large computing and memory resources, particularly in three space dimensions. For $\tilde{N} = 1$, a time marching scheme is obtained from (3.16) with algebraic system

$$(3.17) \quad \mathbf{D}_{\tau,h}^n \mathbf{X}_n = \mathbf{B}_n - \mathbf{C}_{\tau,h}^n \mathbf{X}_{n-1},$$

for $n = 2, \dots, N$ and right-hand side $\mathbf{B}_1 - \mathbf{C}_{\tau,h}^1 \mathbf{V}_0$ for $n = 1$. Our implementation supports a flexible choice of \tilde{N} , as shown in [32]. As the systems already become quite large for small \tilde{N} , particularly in 3D, we restrict ourselves to $\tilde{N} = 1$ in the numerical experiments in Section 5.

- Alternatively, a global variable and time major order of the unknowns can be applied, such that instead of (3.7) the vector of all unknowns is defined by

$$(3.18) \quad \mathbf{X} = (\mathbf{X}^v, \mathbf{X}^p)^\top := (\mathbf{V}_1, \dots, \mathbf{V}_N, \mathbf{P}_1, \dots, \mathbf{P}_N)^\top \in \mathbb{R}^{N \cdot (k+1) \cdot (M^v+M^p)},$$

with \mathbf{V}_n and \mathbf{P}_n of (3.6). This global in time formulation leads to a system matrix with saddle point structure such that block solver techniques, such as Schur complement methods, become feasible. However, the global space-time system comprises a large number of unknowns, necessitating substantial computational resources, particularly in three space dimensions. The approach is not investigated in the present study as well.

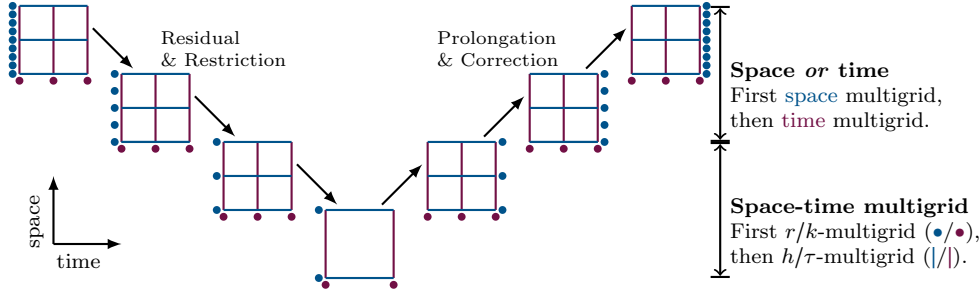


Fig. 1: Sketch of the hp STMG of Algorithm 4.1. The corrections are transferred by the prolongation operators and the residual is transferred by the restriction operators. On each level the error is smoothened by application of the Vanka operator (4.20). The coarsening strategy which is used in Algorithm 4.4, is first in space and then in time in combination with polynomial coarsening before geometric coarsening (cf. (P1), (P2)).

4. Multigrid framework. For solving (3.16) efficiently, we propose an hp space-time multigrid method. For stability reasons, we use the hp STMG method as a preconditioner for GMRES iterations rather than as a solver itself, which has become a standard technique for applying multigrid techniques. For foundational principles of multigrid methods we refer to [21, 9, 47]. Before we present the hp STMG in Algorithm 4.1, that is sketched in Figure 1, we need to define the grid transfer operators, restriction and prolongation, and the smoother.

Let $\{\mathcal{M}_l\}_{l=0}^L$ be a quasi-uniform family of nested triangulations of the interval I into semi-closed subintervals $(t_a, t_b]$ based on *global regular refinement*, with $\mathcal{M}_l = \{I_i = (t_{i,a}, t_{i,b}] \mid i = 1, \dots, N_l^{\text{el}}\}$, for $l = 0, \dots, L$. The finest partition of I is $\mathcal{M}_\tau = \mathcal{M}_L$. For the characteristic mesh size τ_l there holds $\tau_l = \frac{\tau_{l-1}}{2}$, and $\tau_0 = \mathcal{O}(1)$. This results in a hierarchy of nested temporal finite element spaces of type (3.2),

$$(4.1) \quad Y_0^k \subset Y_1^k \subset \dots \subset Y_L^k \subset L^2(0, T).$$

Let further $\{\mathcal{T}_s\}_{s=0}^S$ be a quasi-uniform family of nested triangulations of the spatial domain Ω into (open) quadrilaterals or hexahedrals based on *global regular refinement*, with $\mathcal{T}_s = \{K_i \mid i = 1, \dots, N_s^{\text{el}}\}$, for $s = 0, \dots, S$. The finest partition is $\mathcal{T}_h = \mathcal{T}_S$. For the characteristic mesh size h_s there holds $h_s \approx \frac{h_{s-1}}{2}$ and $h_0 = \mathcal{O}(1)$. This results in a hierarchy of nested spatial finite element spaces of type (3.3),

$$(4.2a) \quad \mathbf{V}_0^{r+1}(\Omega) \subset \mathbf{V}_1^{r+1}(\Omega) \subset \dots \subset \mathbf{V}_S^{r+1}(\Omega) \subset \mathbf{V},$$

$$(4.2b) \quad Q_0^r(\Omega) \subset Q_1^r(\Omega) \subset \dots \subset Q_S^r(\Omega) \subset Q.$$

Similarly to (2.2c), for the nested finite element spaces (4.2b) we define

$$(4.3) \quad Q_s^{r,+} := Q_s^r + \text{span}\{1\}.$$

We put $M_{r+1,s}^v := \dim \mathbf{V}_s^{r+1}$ and $M_{r,s}^p := \dim Q_s^{r,+}$. On the space-time and polynomial order multigrid hierarchy, we define the algebraic tensor product spaces, for $l = 0, \dots, L$ and $s = 0, \dots, S$, as well as $k, r \in \mathbb{N}$ by

$$(4.4) \quad \mathbf{H}_{l,s}^{k,r+1} := Y_l^k(I) \otimes \mathbf{V}_s^{r+1}(\Omega), \quad H_{l,s}^{k,r} := Y_l^k(I) \otimes Q_s^r(\Omega).$$

All spaces, quantities and problems that were introduced before in Section 2 and Section 3 are now studied on the full space-time multigrid hierarchy and for the function spaces (4.4). For this, the respective indices are added in the notation. The grid levels in time and space are denoted by the indices “ l ” and “ s ”, respectively, and the polynomial orders by the indices “ k ” and “ r ”.

4.1. Grid transfer operators. For refinement and coarsening of the space and time mesh, referred to as h -multigrid in our hp STMG, we need to define the grid transfer operators, i.e. restriction and prolongation, for the algebraic tensor product spaces (4.4). We start with the spatial mesh. For the nested finite element spaces (4.2) and (4.3) with bases according to (3.3) we define the isomorphisms which map the degrees of freedom to the finite element spaces as (cf. [37])

$$(4.5a) \quad \mathcal{R}_s^{r+1} : \mathbb{R}^{M_{r+1,s}^v} \rightarrow \mathbf{V}_s^{r+1}, \quad \mathcal{R}_s^{r+1} \mathbf{U}_s = \sum_{i=0}^{M_{r+1,s}^v} U_s^i \chi_{i,s}^v,$$

$$(4.5b) \quad \mathcal{S}_s^r : \mathbb{R}^{M_{r,s}^p} \rightarrow \mathbf{Q}_s^{r,+}, \quad \mathcal{S}_s^r \mathbf{P}_s = \sum_{i=0}^{M_{r,s}^p} P_s^i \chi_{i,s}^p.$$

We note that $\mathbf{Q}_s^r = \{\mathcal{S}_s^r \mathbf{P}_s \mid \mathbf{P}_s \in (M_{h,s}^p \mathbf{1})^\perp\}$ with $\mathbf{1} = (1, \dots, 1)^\top \in \mathbb{R}^{M_{r,s}^p}$ and pressure mass matrix $M_{r,s}^p \in \mathbb{R}^{M_{r,s}^p, M_{r,s}^p}$ of (3.9b). The orthogonality condition $\langle p, \mathbf{1} \rangle_{L^2(\Omega)} = 0$ for $p \in \mathbf{Q}_h^{r,s}$ corresponds to the orthogonality $\langle \mathbf{P}, M_{h,s}^p \mathbf{1} \rangle_{\mathbb{R}^{M_{r,s}^p}} = 0$ for $\mathbf{P} \in \mathbb{R}^{M_{r,s}^p}$. For $s = 0, \dots, S$ and $r \in \mathbb{N}$, we let

$$(4.6) \quad \mathbf{R}_s^{r+1} := \mathbb{R}^{M_{r+1,s}^v} \quad \text{and} \quad \mathbf{S}_s^r := (M_{h,s}^p \mathbf{1})^\perp.$$

For prolongation and restriction in space and with (4.5), we use the canonical choice

$$(4.7a) \quad \begin{aligned} \mathbf{T}_{s-1,s}^r &: \mathbf{R}_{s-1}^{r+1} \times \mathbf{S}_{s-1}^r \rightarrow \mathbf{R}_s^{r+1} \times \mathbf{S}_s^r, \\ \mathbf{T}_{s-1,s}^r &= (\mathcal{R}_s^{r+1})^{-1} \circ \mathcal{R}_{s-1}^{r+1} \times (\mathcal{S}_s^r)^{-1} \circ \mathcal{S}_{s-1}^r, \end{aligned}$$

$$(4.7b) \quad \begin{aligned} \mathbf{T}_{s,s-1}^r &: \mathbf{R}_s^{r+1} \times \mathbf{S}_s^r \rightarrow \mathbf{R}_{s-1}^{r+1} \times \mathbf{S}_{s-1}^r, \\ \mathbf{T}_{s,s-1}^r &= (\mathcal{R}_{s-1}^{r+1})^* \circ ((\mathcal{R}_s^{r+1})^*)^{-1} \times (\mathcal{S}_{s-1}^r)^* \circ ((\mathcal{S}_s^r)^*)^{-1}. \end{aligned}$$

Both operators, $\mathbf{T}_{s-1,s}^r$ and $\mathbf{T}_{s,s-1}^r$, keep the pressure in the correct subspace. For $\mathbf{Z} = (\mathbf{V}, \mathbf{P})^\top \in (\mathbf{R}_{s-1}^{r+1})^{k+1} \times (\mathbf{S}_{s-1}^r)^{k+1}$, with $\mathbf{V} \in (\mathbf{R}_{s-1}^{r+1})^{k+1}$ and $\mathbf{P} \in (\mathbf{S}_{s-1}^r)^{k+1}$, we define the prolongation $\tilde{\mathbf{T}}_{s-1,s}^r : (\mathbf{R}_{s-1}^{r+1})^{k+1} \times (\mathbf{S}_{s-1}^r)^{k+1} \rightarrow (\mathbf{R}_s^{r+1})^{k+1} \times (\mathbf{S}_s^r)^{k+1}$ for the product spaces $(\mathbf{R}_{s-1}^{r+1})^{k+1}$ and $(\mathbf{S}_{s-1}^r)^{k+1}$ by componentwise application of (4.7a),

$$(4.8) \quad \begin{aligned} \tilde{\mathbf{T}}_{s-1,s}^r \mathbf{Z} &:= (\mathbf{T}_{s-1,s}^{r,v} \mathbf{V}^1, \dots, \mathbf{T}_{s-1,s}^{r,v} \mathbf{V}^{k+1}, \mathbf{T}_{s-1,s}^{r,p} \mathbf{P}^1, \dots, \mathbf{T}_{s-1,s}^{r,p} \mathbf{P}^{k+1})^\top \\ &= \begin{pmatrix} \mathbf{E}_{k+1} \otimes \mathbf{T}_{s-s,s}^{r,v} & \mathbf{0} \\ \mathbf{0} & \mathbf{E}_{k+1} \otimes \mathbf{T}_{s-1,s}^{r,p} \end{pmatrix} \begin{pmatrix} \mathbf{V} \\ \mathbf{P} \end{pmatrix}, \end{aligned}$$

where $\mathbf{T}_{s-1,s}^{r,v} : \mathbf{R}_{s-1}^{r+1} \rightarrow \mathbf{R}_s^{r+1}$ and $\mathbf{T}_{s-1,s}^{r,p} : \mathbf{S}_{s-1}^r \rightarrow \mathbf{S}_s^r$ are the velocity and pressure parts of the prolongation $\mathbf{T}_{s,s-1}^r$ defined in (4.7a). The corresponding restriction operator $\tilde{\mathbf{T}}_{s,s-1}^r : (\mathbf{R}_s^{r+1})^{k+1} \times (\mathbf{S}_s^r)^{k+1} \rightarrow (\mathbf{R}_{s-1}^{r+1})^{k+1} \times (\mathbf{S}_{s-1}^r)^{k+1}$ is defined analogously by

$$(4.9) \quad \begin{aligned} \tilde{\mathbf{T}}_{s,s-1}^r \mathbf{Z} &:= (\mathbf{T}_{s,s-1}^{r,v} \mathbf{V}^1, \dots, \mathbf{T}_{s,s-1}^{r,v} \mathbf{V}^{k+1}, \mathbf{T}_{s,s-1}^{r,p} \mathbf{P}^1, \dots, \mathbf{T}_{s,s-1}^{r,p} \mathbf{P}^{k+1})^\top \\ &= \begin{pmatrix} \mathbf{E}_{k+1} \otimes \mathbf{T}_{s,s-1}^{r,v} & \mathbf{0} \\ \mathbf{0} & \mathbf{E}_{k+1} \otimes \mathbf{T}_{s,s-1}^{r,p} \end{pmatrix} \begin{pmatrix} \mathbf{V} \\ \mathbf{P} \end{pmatrix}, \end{aligned}$$

where $\mathbf{T}_{s,s-1}^{r,v} : \mathbf{R}_s^{r+1} \rightarrow \mathbf{R}_{s-1}^{r+1}$ and $\mathbf{T}_s^{r,p} : \mathbf{S}_s^r \rightarrow \mathbf{S}_{s-1}^r$ are the velocity and pressure parts of the restriction $\mathbf{T}_{s,s-1}^r$ defined in (4.7b). For global vectors $\mathbf{Z} = (\mathbf{Z}_1 \dots, \mathbf{Z}_{N_l})^\top \in ((\mathbf{R}_{s-1}^{r+1})^{k+1} \times (\mathbf{S}_{s-1}^r)^{k+1})^{N_l}$ with $\mathbf{Z}_n = (\mathbf{V}_n, \mathbf{P}_n)^\top \in (\mathbf{R}_{s-1}^{r+1})^{k+1} \times (\mathbf{S}_{s-1}^r)^{k+1}$, for $n = 1, \dots, N_l$, and with $\mathbf{1}_{N_l} := (1, \dots, 1) \in \mathbb{R}^{N_l}$ according to (3.5) to (3.7), prolongation and restriction are then defined by

$$(4.10) \quad \overline{\mathbf{T}}_{s-1,s}^r \mathbf{Z} := ((\mathbf{1}_{N_l} \otimes \tilde{\mathbf{T}}_{s-1,s}^r) \mathbf{Z})^\top \quad \text{and} \quad \overline{\mathbf{T}}_{s,s-1}^r \mathbf{Z} := ((\mathbf{1}_{N_l} \otimes \tilde{\mathbf{T}}_{s,s-1}^r) \mathbf{Z})^\top.$$

Next, we introduce the grid transfer operator for the hierarchy of temporal meshes. Similarly to (4.5), for temporal mesh level $l = 0, \dots, L$ we define the isomorphism, on spatial mesh level $s = 0, \dots, S$, with $D_{l,s}^{k,r} := N_l(k+1)(M_{r+1,s}^v + M_{r,s}^p)$ as

$$(4.11) \quad \mathcal{I}_l^k : \mathbb{R}^{D_{l,s}^{k,r}} \rightarrow Y_l^k(I) \otimes \mathbb{R}^{M_{r+1,s}^v + M_{r,s}^p}, \quad \mathcal{I}_l^k \mathbf{W} = \sum_{n=1}^{N_l} \sum_{a=1}^{k+1} \begin{pmatrix} \mathbf{W}_{n,a}^{l,v} \\ \mathbf{W}_{n,a}^{l,p} \end{pmatrix} \varphi_{n,a}^l.$$

Here, we substructured \mathbf{W} according to

$$(4.12) \quad \mathbf{W} = \left(\mathbf{W}_{1,1}^{l,v}, \dots, \mathbf{W}_{1,k+1}^{l,v}, \mathbf{W}_{1,1}^{l,p}, \dots, \mathbf{W}_{1,k+1}^{l,p}, \dots, \mathbf{W}_{N_l,1}^{l,v}, \dots, \mathbf{W}_{N_l,k+1}^{l,v}, \mathbf{W}_{N_l,1}^{l,p}, \dots, \mathbf{W}_{N_l,k+1}^{l,p} \right)^\top,$$

with $\mathbf{W}_{n,a}^{l,v} \in \mathbb{R}^{M_{r+1,s}^v}$ and $\mathbf{W}_{n,a}^{l,p} \in \mathbb{R}^{M_{r,s}^p}$ for $n = 1, \dots, N_l$ and $a = 1, \dots, k+1$. For prolongation and restriction we use the canonical choices again,

$$(4.13a) \quad \mathbf{I}_{l-1,l}^k : \mathbb{R}^{D_{l-1,s}^{k,r}} \rightarrow \mathbb{R}^{D_{l,s}^{k,r}}, \quad \mathbf{I}_{l-1,l}^k = (\mathcal{I}_l^k)^{-1} \circ \mathcal{I}_{l-1}^k,$$

$$(4.13b) \quad \mathbf{I}_{l,l-1}^k : \mathbb{R}^{D_{l,s}^{k,r}} \rightarrow \mathbb{R}^{D_{l-1,s}^{k,r}}, \quad \mathbf{I}_{l,l-1}^k = (\mathcal{I}_{l-1}^k)^* \circ ((\mathcal{I}_l^k)^*)^{-1}.$$

Space-time prolongation $\mathbf{T}_{l-1,l;s-1,s}^{k,r} : \mathbb{R}^{D_{l-1,s-1}^{k,r}} \rightarrow \mathbb{R}^{D_{l,s}^{k,r}}$ and restriction $\mathbf{T}_{l,l-1;s,s-1}^{k,r} : \mathbb{R}^{D_{l,s}^{k,r}} \rightarrow \mathbb{R}^{D_{l-1,s-1}^{k,r}}$ are then defined by the concatenation of $\mathbf{I}_{l-1,l}^k$ and $\overline{\mathbf{T}}_{s-1,s}^r$ and of $\mathbf{I}_{l,l-1}^k$ and $\overline{\mathbf{T}}_{s,s-1}^r$, respectively, as

$$(4.14) \quad \mathbf{T}_{l-1,l;s-1,s}^{k,r} := \mathbf{I}_{l-1,l}^k \circ \overline{\mathbf{T}}_{s-1,s}^r \quad \text{and} \quad \mathbf{T}_{l,l-1;s,s-1}^{k,r} := \mathbf{I}_{l,l-1}^k \circ \overline{\mathbf{T}}_{s,s-1}^r.$$

Remark 4.1. If a time marching process according to (3.17) is applied, we omit h -multigrid in time by solving (3.17) on the finest time mesh \mathcal{M}_L . There, we perform hp -multigrid in space and p -multigrid in time. In (4.14), the operators $\mathbf{I}_{l-1,l}^k$ and $\mathbf{I}_{l,l-1}^k$ then become the identities. Under this assumption, the hp STMG (Algorithm 4.1) is still well-defined. This also applies to macro time steps (cf. Remark 3.3) by coupling $\tilde{N} < N$ systems (3.17).

For the coarsening and prolongation of the polynomial degrees $k, r \in \mathbb{N}$ of the discrete spaces (4.4), referred to as p -multigrid in the hp multigrid context, we need to define corresponding grid transfer operators. For simplicity, we assume for (4.4) that

$$(4.15) \quad k = 2^K \quad \text{for some } K \in \mathbb{N}, \quad r = 2^R \quad \text{for some } R \in \mathbb{N}.$$

As we halve the polynomial orders $k, r \in \mathbb{N}$ for restriction, i.e. $k \mapsto \lfloor k/2 \rfloor$ (bisection), and double it for prolongation, we would otherwise need to maintain an accounting

vector for the polynomial orders due to the noninvertibility of the floor function. This overhead in notation is avoided in this section by (4.15). The general case of arbitrary $k, r \in \mathbb{N}$ is addressed in Algorithm 4.3. The coarsening strategy for the polynomial degrees is motivated by computational studies, which have demonstrated that this approach strikes a favorable balance between two-level ($k \mapsto 1$) and decrease by one ($k \mapsto k - 1$) coarsening. We also refer to [17, Section 3.2.2] for a review of polynomial coarsening strategies. For prolongation of the spatial polynomial order r , i.e. $\frac{r}{2} \mapsto r$ in (4.2), and restriction, i.e. $r \mapsto \frac{r}{2}$, we let the transfer operators (for $R \geq 2$)

$$(4.16) \quad \mathbf{T}_s^{\frac{r}{2}, r} : \mathbf{R}_s^{\frac{r}{2}} \times \mathbf{S}_s^{\frac{r}{2}-1} \rightarrow \mathbf{R}_s^r \times \mathbf{S}_s^{r-1}, \quad \mathbf{T}_s^{r, \frac{r}{2}} : \mathbf{R}_s^r \times \mathbf{S}_s^{r-1} \rightarrow \mathbf{R}_s^{\frac{r}{2}} \times \mathbf{S}_s^{\frac{r}{2}-1}$$

for the spaces (4.6) be defined analogously to (4.7) along with (4.5). The prolongation $\overline{\mathbf{T}}_s^{\frac{r}{2}, r}$ and restriction $\overline{\mathbf{T}}_s^{r, \frac{r}{2}}$ extend $\mathbf{T}_s^{\frac{r}{2}, r}$ and $\mathbf{T}_s^{r, \frac{r}{2}}$ to the global vector of unknowns (4.12) along the lines of (4.8) and (4.9). Finally, we define the prolongation and restriction of the temporal polynomial order k in (4.1). For prolongation and restriction in time of the p -multigrid method,

$$(4.17) \quad \mathbf{I}_l^{\frac{k}{2}, k} : \mathbb{R}^{D_{l,s}^{\frac{k}{2}, r}} \rightarrow \mathbb{R}^{D_{l,s}^{k, r}}, \quad \mathbf{I}_l^{k, \frac{k}{2}} : \mathbb{R}^{D_{l,s}^{k, r}} \rightarrow \mathbb{R}^{D_{l,s}^{\frac{k}{2}, r}}$$

are defined analogously to (4.13) along with (4.11). Space-time combined grid transfer operations of the p -multigrid method are then constructed by concatenation of the operators in (4.16) and (4.17), similarly to (4.14), such that

$$(4.18) \quad \mathbf{T}_{l,s}^{\frac{k}{2}, k; \frac{r}{2}, r} := \mathbf{I}_l^{\frac{k}{2}, k} \circ \overline{\mathbf{T}}_s^{\frac{r}{2}, r} \quad \text{and} \quad \mathbf{T}_{l,s}^{k, \frac{k}{2}; r, \frac{r}{2}} := \mathbf{I}_l^{k, \frac{k}{2}} \circ \overline{\mathbf{T}}_s^{r, \frac{r}{2}}.$$

4.2. Space-time Vanka smoother. The smoother for approximating the solutions of the linear systems on the multigrid levels is a further building block of multigrid techniques. It aims at smoothing out high frequency errors in the solutions to the linear systems

$$(4.19) \quad \mathbf{S}_{l,s}^{k, r} \mathbf{X}_{l,s}^{k, r} = \mathbf{B}_{l,s}^{k, r}$$

on the hp multigrid hierarchy. On the finest hp multigrid level, (4.19) recasts the linear system of Problem 3.2 in its algebraic form. On the coarser levels, the right-hand side in (4.19) corresponds to residuals and the solution to corrections. The V -cycle hp multigrid iteration is outlined in detail in Subsection 4.3 and in Algorithm 4.1. The smoothing operation is done by a simple iteration

$$\text{smoother}(\mathbf{S}_{l,s}^{k, r}, \mathbf{B}_{l,s}^{k, r}) \approx (\mathbf{S}_{l,s}^{k, r})^{-1} \mathbf{B}_{l,s}^{k, r},$$

and reduces the high frequency components of the residual $\mathbf{B}_{l,s}^{k, r} - \mathbf{S}_{l,s}^{k, r} \mathbf{X}_{l,s}^{k, r}$. The linear (optimal) complexity of the geometric multigrid method is achieved when the reduction rate of the residual is constant across levels. In our implementation we use a space-time cell wise Vanka smoother. For a detailed description in the STFEM we refer to [4, 5] and the references therein. For the local (time-stepping) approach (3.17), the Vanka smoother is built for all $(k+1) \cdot (M_{r+1,s}^v + M_{r,s}^p)$ degrees of freedom of a space-time element which amounts to a block size of $(k+1)(d(r+2)^d + (r+1)^d)$, with space dimension d . We use an inner direct solver. For macro time steps and the global in time approach (cf. Remark 3.3) the Vanka smoother is assembled over the

subintervals, which increases the block size. More precisely, on the space-time mesh $T_h \otimes \mathcal{M}_\tau$ the Vanka smoother is defined, for $\mathbf{S} := \mathbf{S}_{l,s}^{k,r}$ and $\mathbf{b} := \mathbf{B}_{l,s}^{k,r}$, by

$$(4.20) \quad \text{smoother}(\mathbf{S}, \mathbf{b}) = \left(\sum_{T \in T_h \otimes \mathcal{M}_\tau} \mathbf{R}_T^\top [\mathbf{R}_T \mathbf{S}_T \mathbf{R}_T^\top]^{-1} \mathbf{R}_T \right) \mathbf{b},$$

where \mathbf{R}_T is the restriction to those nodes that belong to the space-time mesh element $T \in T_h \otimes \mathcal{M}_\tau$ and \mathbf{S}_T is the corresponding local system matrix on T . For their definition we refer to [4, 5]. The smoother is computationally expensive, and its application has the cellwise complexity of $O((k+1)^2(d(r+2)^d + (r+1)^d)^2)$. With a relaxation parameter $\omega_\ell \in (0, 1)$, a smoother iteration (cf. Algorithm 4.1) is then given by

$$(4.21) \quad \text{Smoother}(\mathbf{S}, \mathbf{b}, \mathbf{u}) = \mathbf{u} + \omega \text{smoother}(\mathbf{S}, \mathbf{b} - \mathbf{S}\mathbf{u}).$$

Our current implementation of the smoother does not take full advantage of the block structure arising from the tensor-product STFEM. The block structure is used to avoid the assembly of the space-time system matrix. We will leverage the block structure to improve the smoother efficiency in future work.

4.3. The hp space-time multigrid method. We introduce our V-cycle hp space-time multigrid approach for tensor-product STFEMs. We assume that the linear system of Problem 3.2 is represented on the multigrid levels $l = 0, \dots, L$ and $s = 0, \dots, S$ and for the polynomial degrees $k, r \in \mathbb{N}$ by (4.19). While $k = 0, r = 0$ is theoretically possible, we exclude this due to the suboptimal performance in practice. For ease of presentation, we assume, without loss of generality, that $S \geq L$ and $r \geq k$. This is a reasonable condition for FEM flow simulations that are often characterized by dominating dynamics in the spatial variables. The hp STMG for (4.19) is outlined in Algorithm 4.1 and sketched in Figure 1. We recall that the hp STMG is used as a preconditioner for GMRES iterations to (4.19).

Algorithm 4.1 hp space time multigrid algorithm for Problem 3.2.

Start. System $\mathbf{S}_{l,s}^{k,r} \mathbf{X}_{l,s}^{k,r} = \mathbf{B}_{l,s}^{k,r}$, multigrid levels $0 \leq l \leq L, 0 \leq s \leq S$, polynomial orders $k \leq r$, smoothing steps ν_1, ν_2 , smoother $\mathbf{W}_{l,s}^{k,r}$.

1. Presmoothing. Given an initial guess $\mathbf{X}_{l,s}^{k,r;0} \in \mathbb{R}^{D_{l,s}^{k,r}}$, compute $\mathbf{X}_{l,s}^{k,r;\nu_0}$ by ν_1 linear smoothing steps as

$$(4.22) \quad \mathbf{X}_{l,s}^{k,r;\nu+1} = \mathbf{X}_{l,s}^{k,r} - (\mathbf{W}_{l,s}^{k,r})^{-1} (\mathbf{S}_{l,s}^{k,r} \mathbf{X}_{l,s}^{k,r;\nu} - \mathbf{B}_{l,s}^{k,r}), \quad \text{for } \nu = 0, \dots, \nu_1 - 1.$$

2. Coarse grid correction (p -multigrid). If $r > K$ then restrict the residual

$$(4.23) \quad \mathbf{B}_{l,s}^{k,\frac{r}{2}} = \mathbf{T}_{l,s}^{k,k;r,\frac{r}{2}} (\mathbf{B}_{l,s}^{k,r} - \mathbf{S}_{l,s}^{k,r} \mathbf{X}_{l,s}^{k,r;\nu_1}),$$

and let $\mathbf{Y}_{l,s}^{k,\frac{r}{2}} \in \mathbb{R}^{D_{l,s}^{k,\frac{r}{2}}}$ satisfy

$$(4.24) \quad \mathbf{S}_{l,s}^{k,\frac{r}{2}} \mathbf{Y}_{l,s}^{k,\frac{r}{2}} = \mathbf{B}_{l,s}^{k,\frac{r}{2}}.$$

Else restrict the residual

Continued Algorithm 4.1

$$(4.25) \quad \mathbf{B}_{l,s}^{k, \frac{k}{2}; r, \frac{r}{2}} = \mathbf{T}_{l,s}^{k, \frac{k}{2}; r, \frac{r}{2}} (\mathbf{B}_{l,s}^{k,r} - \mathbf{S}_{l,s}^{k,r} \mathbf{X}_{l,s}^{k,r; \nu_1}),$$

and let $\mathbf{Y}_{l,s}^{k, \frac{k}{2}; r, \frac{r}{2}} \in \mathbb{R}^{D_{l,s}^{k, \frac{k}{2}; r, \frac{r}{2}}}$ satisfy

$$(4.26) \quad \mathbf{S}_{l,s}^{k, \frac{k}{2}; r, \frac{r}{2}} \mathbf{Y}_{l,s}^{k, \frac{k}{2}; r, \frac{r}{2}} = \mathbf{B}_{l,s}^{k, \frac{k}{2}; r, \frac{r}{2}}.$$

If $r = 2$, continue to step 3, else if $r > 2$, compute an approximation to $\mathbf{Y}_{l,s}^{k; \frac{r}{2}}$ or $\mathbf{Y}_{l,s}^{\frac{k}{2}; \frac{r}{2}}$, by one step of the p -multigrid algorithm at polynomial degree $\frac{r}{2}$ to (4.24) or (4.26) with initial guess $\mathbf{Y}_{l,s}^{k, \frac{r}{2}; 0} = \mathbf{0}$ or $\mathbf{Y}_{l,s}^{\frac{k}{2}, \frac{r}{2}; 0} = \mathbf{0}$, respectively.

3. Coarse grid correction of h -multigrid. If $s > L$, restrict the residual

$$(4.27) \quad \mathbf{B}_{l,s-1}^{1,1} = \mathbf{T}_{l,l;s,s-1}^{1,1} (\mathbf{B}_{l,s}^{1,1} - \mathbf{S}_{l,s}^{1,1} \mathbf{Y}_{l,s}^{1,1}),$$

and let $\mathbf{Y}_{l,s-1}^{1,1} \in \mathbb{R}^{D_{l,s-1}^{1,1}}$ satisfy

$$(4.28) \quad \mathbf{S}_{l,s-1}^{1,1} \mathbf{Y}_{l,s-1}^{1,1} = \mathbf{B}_{l,s-1}^{1,1}.$$

Else restrict the residual

$$(4.29) \quad \mathbf{B}_{l-1,s-1}^{1,1} = \mathbf{T}_{l,l-1;s,s-1}^{1,1} (\mathbf{B}_{l,s}^{1,1} - \mathbf{S}_{l,s}^{1,1} \mathbf{X}_{l,s}^{1,1; \nu_1}),$$

and let $\mathbf{Y}_{l-1,s-1}^{1,1} \in \mathbb{R}^{D_{l-1,s-1}^{1,1}}$ satisfy

$$(4.30) \quad \mathbf{S}_{l-1,s-1}^{1,1} \mathbf{Y}_{l-1,s-1}^{1,1} = \mathbf{B}_{l-1,s-1}^{1,1}.$$

If $s = 2$, solve (4.30), else if $s > 2$, compute an approximation to $\mathbf{Y}_{l,s-1}^{1,1}$ or $\mathbf{Y}_{l-1,s-1}^{1,1}$, by applying one step of the h -multigrid algorithm at level $s - 1$ to (4.28) or (4.30) with initial guess $\mathbf{Y}_{l,s-1}^{1,1; 0} = \mathbf{0}$ or $\mathbf{Y}_{l-1,s-1}^{1,1; 0} = \mathbf{0}$, respectively.

If $r = 1$,

if $s \leq L$, set

$$(4.31) \quad \mathbf{X}_{l,s}^{1,1; \nu_1+1} = \mathbf{X}_{l,s}^{1,1; \nu_1} + \mathbf{T}_{l-1,l;s-1,s}^{1,1} \mathbf{Y}_{l-1,s-1}^{1,1},$$

else set

$$(4.32) \quad \mathbf{X}_{l,s}^{1,1; \nu_1+1} = \mathbf{X}_{l,s}^{1,1; \nu_1} + \mathbf{T}_{l,l;s-1,s}^{1,1} \mathbf{Y}_{l-1,s-1}^{1,1},$$

else if $r \leq K$, set

$$(4.33) \quad \mathbf{X}_{l,s}^{k,r; \nu_1+1} = \mathbf{X}_{l,s}^{k,r; \nu_1} + \mathbf{T}_{l,s}^{k, k; \frac{r}{2}, r} \mathbf{Y}_{l,s}^{\frac{k}{2}, \frac{r}{2}},$$

else set

$$(4.34) \quad \mathbf{X}_{l,s}^{k,r; \nu_1+1} = \mathbf{X}_{l,s}^{k,r; \nu_1} + \mathbf{T}_{l,s}^{k, k; \frac{r}{2}, r} \mathbf{Y}_{l,s}^{k, \frac{r}{2}}.$$

4. Postsmoothing. Compute $\mathbf{X}_{l,s}^{k,r; \nu_1+\nu_2+1} \in \mathbb{R}^{D_{l,s}^{k,r}}$ by ν_2 linear smoothing steps

$$(4.35) \quad \mathbf{X}_{l,s}^{k,r; \nu+1} = \mathbf{X}_{l,s}^{k,r} - (\mathbf{W}_{l,s}^{k,r})^{-1} (\mathbf{S}_{l,s}^{k,r} \mathbf{X}_{l,s}^{k,r; \nu} - \mathbf{B}_{l,s}^{k,r}), \quad \text{for } \nu = \nu_1 + 1, \dots, \nu_1 + \nu_2.$$

Set $\mathbf{X}_{l,s}^{k,r; \nu_1+\nu_2+1}$ as the solution of one iteration of the V -cycle hp multigrid algorithm.

Algorithm 4.3 CONSTRUCTHIERARCHY(h_L, h_0, r_L, r_0)**Require:** Fine and coarse mesh size h_L, h_0 , polynomial degrees r_L, r_0 .

- 1: $\mathcal{H} \leftarrow ()$, $h \leftarrow h_{L_g}$, $r \leftarrow r_L$
- 2: **while** $r \geq r_0$ **do**
- 3: $\mathcal{H} \leftarrow (h, r) \times \mathcal{H}$ ▶ Polynomial coarsening
- 4: $r \leftarrow \lfloor r/2 \rfloor$ ▶ halve polynomial degree
- 5: **while** $h \leq h_0$ **do**
- 6: $\mathcal{H} \leftarrow (h, r) \times \mathcal{H}$ ▶ Geometric coarsening
- 7: $h \leftarrow 2h$ ▶ Coarsen triangulation (“double mesh size” for simplicity)
- 8: **return** \mathcal{H}

Algorithm 4.4 COMBINEHIERARCHIES($\mathcal{H}_h, \mathcal{H}_\tau$)**Require:** Spatial hierarchy obtained by Algorithm 4.3: $\mathcal{H}_h = ((h_\ell, p_\ell))_{\ell=1}^S$ **Require:** Temporal hierarchy obtained by Algorithm 4.3: $\mathcal{H}_\tau = ((\tau_\ell, k_\ell))_{\ell=1}^{\mathcal{L}}$

- 1: $\mathcal{H}_{st} \leftarrow ()$, $(\tau_{\text{pad}}, k_{\text{pad}}) \leftarrow \mathcal{H}_\tau[\mathcal{L}]$
- 2: **for** $\ell = \mathcal{L} + 1$ to \mathcal{L}_{max} **do**
- 3: $\mathcal{H}_\tau \leftarrow \mathcal{H}_\tau \times (\tau_{\text{pad}}, k_{\text{pad}})$ ▶ Pad the hierarchy to length \mathcal{L}_{max}
- 4: **for** $\ell = 1$ to \mathcal{L}_{max} **do**
- 5: Let $(\tau_\ell, k_\ell) \leftarrow \mathcal{H}_\tau[\ell]$, $(h_\ell, r_\ell) \leftarrow \mathcal{H}_h[\ell]$ ▶ Combine level by level
- 6: $\mathbf{H}_{\ell_\ell, s_\ell}^{k_\ell, r_\ell} := Y_{\ell_\ell}^{k_\ell}(I) \otimes \mathbf{V}_{s_\ell}^{r_\ell+1}(\Omega)$, $H_{\ell_\ell, s_\ell}^{k_\ell, r_\ell} := Y_{\ell_\ell}^{k_\ell}(I) \otimes Q_{s_\ell}^{r_\ell}(\Omega)$
- 7: $\mathcal{H}_{st} \leftarrow \mathcal{H}_{st} \times (\mathbf{H}_{\ell_\ell, s_\ell}^{k_\ell, r_\ell}, H_{\ell_\ell, s_\ell}^{k_\ell, r_\ell})$
- 8: **return** \mathcal{H}_{st}

4.4. Multigrid Sequence Generation. Finally, we still comment on some implementational aspects for Algorithm 4.1. We construct the space-time multigrid hierarchy by coarsening sequences of spatial and temporal finite element spaces, which are combined by tensor products, according to two guiding principles:

- (P1) **Spatial Coarsening over Temporal Coarsening:** Perform geometric coarsening first in the spatial dimension, then in the temporal dimension.
- (P2) **Polynomial over Geometric Coarsening:** Apply coarsening in polynomial degrees (r/k) before geometric coarsening (h/τ).

Following (P2), the sequences of nested temporal and spatial finite element spaces are generated through Algorithm 4.3. We generate a temporal hierarchy of finite element spaces $Y_l^k(I)$ (cf. (4.1)) with geometric level l and polynomial degree k . Let L be the number of geometric levels in time, and $\lfloor \log_2(k) \rfloor$ the number of polynomial levels. Thus, the number of temporal levels is $\mathcal{L} := L + \lfloor \log_2(k) \rfloor$. The spatial hierarchy of finite element spaces $\mathbf{V}_s^{r+1}(\Omega)$, $Q_s^r(\Omega)$ on geometric level s with polynomial degree r (cf. (4.2)) is generated analogously. Let S be the number of geometric levels in space, and $\lfloor \log_2(r) \rfloor$ the number of polynomial levels. Thus, the number of spatial levels is $\mathcal{S} := S + \lfloor \log_2(r) \rfloor$. These two hierarchies are merged into a single STMG sequence of size $\mathcal{L}_{\text{max}} = \max(\mathcal{L}, \mathcal{S})$. If $\mathcal{L} < \mathcal{L}_{\text{max}}$, we pad the final temporal spaces to match the finer levels in time, setting $Y_m^k(I) = Y_{\mathcal{L}}^k(I)$, $m = L + 1, \dots, S$ (cf. Algorithm 4.4 line 3). If $\mathcal{S} < \mathcal{L}_{\text{max}}$, an analogous padding applies to $\mathbf{V}_m^{r+1}(\Omega)$ and $Q_m^r(\Omega)$ if $\mathcal{L} > \mathcal{S}$. For a level $\ell \in \{1, \dots, \mathcal{L}_{\text{max}}\}$, we denote ℓ_ℓ and s_ℓ as the temporal and spatial geometric level, k_ℓ and r_ℓ as the temporal and spatial polynomial degree. Following (P1), the space-time finite element spaces $\mathbf{H}_{\ell_\ell, s_\ell}^{k_\ell, r_\ell+1}$ and $H_{\ell_\ell, s_\ell}^{k_\ell, r_\ell}$, where $\ell \in \{1, \dots, \mathcal{L}_{\text{max}}\}$, are generated in Algorithm 4.4 line 7. According to the construction in Algorithm 4.4 and 4.3, the

spaces are ordered such that the coarsest space-time function space, characterized by large h , τ and small p , k , is located at $\ell = 0$. Two additional principles for the generation of the multigrid hierarchy naturally arise from Algorithm 4.4 and 4.3.

- (P3) **True Space-Time Multigrid at Coarsest Level:** Levels with space-time coarsening are put at the lower levels of the hierarchy.
- (P4) **Padding for Pure Space or Time Level:** Padding with identical function spaces is done at the finer levels.

For an example of a generated Multigrid sequence, we refer to Appendix A. Although placing full space-time levels at the top of the multigrid hierarchy could more rapidly reduce the total number of space-time degrees of freedom, they are placed according to (P3). This choice is guided by a CFL-type condition that is derived in [10] for one-dimensional space-time multigrid approaches to the heat equation, which ensures convergence under space-time coarsening. Numerical experiments indicate that such a condition also arises for the Stokes system: adopting “early” space-time coarsening at the top of the hierarchy can degrade the performance of multigrid methods for STFEMs.

4.5. Matrix-free operator evaluation. In this work, linear operators are evaluated without the explicit formation and storage of system matrices. For this, we rely on the matrix-free multigrid framework in the `deal.II` library [2, 28, 35, 17]. A matrix-vector product $\mathbf{Y} = \mathbf{S}\mathbf{X}$ (cf. (4.19)) is computed via global accumulation of local element-wise operations,

$$\mathbf{S}\mathbf{X} = \sum_{c=1}^{n_c} \mathbf{R}_{c,\text{loc-glob}}^\top \mathbf{S}_c \mathbf{R}_{c,\text{loc-glob}} \mathbf{X}, \quad \mathbf{S}_c = \mathbf{B}_c^\top \mathbf{D}_c \mathbf{B}_c,$$

where $\mathbf{R}_{c,\text{loc-glob}}$ maps local degrees of freedom to global indices, \mathbf{B}_c contains shape function gradients, and \mathbf{D}_c encodes quadrature weights and material coefficients. Sum-factorization then reduces the multi-dimensional operations to a product of one-dimensional operations. Vectorization further accelerates the evaluations.

These techniques are used to assemble matrix-vector products with the spatial operators in (3.9). The temporal matrices in (3.8) are precomputed as described in [32]. Products of the form $\mathbf{M}^\top \otimes \mathbf{A}_h \mathbf{u}$ are evaluated by computing $\mathbf{A}_h \mathbf{u}^i$ once for each temporal degree of freedom, followed by a matrix-vector multiplication with the temporal matrices in a blockwise sense (cf. [32]). This approach extends naturally to all Kronecker products in (3.14).

5. Numerical experiments. We validate the accuracy and convergence properties of the proposed hp STMG solver for the Stokes system using a sequence of polynomial degrees and mesh refinements. We use inf-sup stable $\mathbb{Q}_{r+1}/\mathbb{P}_r^{\text{disc}}$ elements in space and a DG(k) discretization in time. To solve the linear systems of equations, we use a GMRES method with a single V-cycle hp STMG preconditioning step per iteration. To ensure efficiency and scalability, the number of iterations until convergence is reached must remain bounded as the mesh size h is reduced or the polynomial degree r is increased. Thus, we characterize the solver’s performance in terms of:

h -robustness: Iteration counts remain bounded independently of the mesh size h .

p -robustness: Iteration counts remain bounded independently of the degree p .

Robustness is important to ensure that the computational cost increases linearly with the problem size, preserving the computational complexity.

The tests were performed on an HPC cluster (HSUper at HSU) with 571 nodes, each with 2 Intel Xeon Platinum 8360Y CPUs and 256 GB RAM. The processors have

36 cores each and the number of MPI processes always match the cores. As mentioned in Remark 3.3, we restrict ourselves to $\tilde{N} = 1$, for computational studies with $\tilde{N} > 1$ we refer to [32].

Table 1: Calculated errors of the velocity and pressure in the space-time L^2 -norm and experimental order of convergence (eoc) for $\mathbb{Q}_{r+1}^2/\mathbb{P}_r^{\text{disc}}/\text{DG}(r)$ discretizations of the Stokes system for (5.1a).

h	$r = 4$				$r = 5$			
	e_{L^2/L^2}^v	eoc	e_{L^2/L^2}^p	eoc	e_{L^2/L^2}^v	eoc	e_{L^2/L^2}^p	eoc
2^{-1}	$1.003 \cdot 10^{-4}$	-	$1.149 \cdot 10^{-3}$	-	$2.711 \cdot 10^{-5}$	-	$1.016 \cdot 10^{-3}$	-
2^{-2}	$2.327 \cdot 10^{-6}$	5.43	$1.115 \cdot 10^{-4}$	3.36	$2.281 \cdot 10^{-7}$	6.89	$1.406 \cdot 10^{-5}$	6.18
2^{-3}	$3.981 \cdot 10^{-8}$	5.87	$3.586 \cdot 10^{-6}$	4.96	$1.877 \cdot 10^{-9}$	6.92	$2.299 \cdot 10^{-7}$	5.93
2^{-4}	$6.392 \cdot 10^{-10}$	5.96	$1.126 \cdot 10^{-7}$	4.99	$1.590 \cdot 10^{-11}$	6.88	$3.885 \cdot 10^{-9}$	5.89
2^{-5}	$1.108 \cdot 10^{-11}$	5.85	$3.751 \cdot 10^{-9}$	4.91	$3.529 \cdot 10^{-12}$	2.17	$1.175 \cdot 10^{-9}$	1.73

Table 2: Number of GMRES iterations until convergence for different polynomial degrees r and number of refinements c with $\mathbb{Q}_{r+1}^2/\mathbb{P}_r^{\text{disc}}/\text{DG}(r)$ discretization of the Stokes system and for hp STMG (left) and h -multigrid in space method (right).

$r \setminus c$	1	2	3	4	5	6	$r \setminus c$	1	2	3	4	5	6
2	14.0	15.0	15.0	14.0	13.0	10.6	2	14.0	15.0	15.0	14.0	13.0	10.6
3	19.8	15.9	16.0	15.0	13.7	11.0	3	19.0	17.9	18.9	18.3	16.4	14.0
4	27.8	23.0	22.9	21.9	19.0	15.5	4	24.0	26.8	24.7	24.6	21.4	18.4
5	31.0	26.4	26.6	22.8	18.7	14.9	5	26.0	26.4	28.8	27.7	24.7	21.9
6	45.0	36.1	36.7	29.0	23.1	17.2	6	35.0	33.9	34.6	30.9	29.6	26.9
7	50.8	43.8	42.8	32.8	25.6	19.6	7	40.0	38.8	39.6	36.7	34.5	31.9

5.1. Convergence test. As a first test case, we consider a model problem on the space-time domain $\Omega \times I = [0, 1]^2 \times [0, 1]$ with prescribed solution given for the velocity $\mathbf{v}: \Omega \times I \rightarrow \mathbb{R}^2$ and pressure $p: \Omega \times I \rightarrow \mathbb{R}$ by

$$(5.1a) \quad \mathbf{v}(\mathbf{x}, t) = \sin(t) \begin{pmatrix} \sin^2(\pi x) \sin(\pi y) \cos(\pi y) \\ \sin(\pi x) \cos(\pi x) \sin^2(\pi y) \end{pmatrix},$$

$$(5.1b) \quad p(\mathbf{x}, t) = \sin(t) \sin(\pi x) \cos(\pi x) \sin(\pi y) \cos(\pi y).$$

We set the kinematic viscosity to $\nu = 0.1$ and choose the external force \mathbf{f} such that the solution (5.1) satisfies (2.1). The initial velocity is prescribed as zero and homogeneous Dirichlet boundary conditions are imposed on $\partial\Omega$ for all times

$$\mathbf{v} = \mathbf{0} \text{ on } \Omega \times \{0\}, \quad \mathbf{v} = \mathbf{0}, \text{ on } \partial\Omega \times (0, T].$$

The space-time mesh $\mathcal{T}_h \otimes \mathcal{M}_\tau$ is a uniform triangulation of the space-time domain $\Omega \times I$. We use discretizations with varying polynomial degrees $r \in \{3, 4, \dots, 8\}$ in space and $k = r$ in time to test the convergence.

Table 1 shows the findings of our convergence study for $r \in \{4, 5\}$. The expected orders of convergence match with the experimental orders. For a full account of all tests, we refer to Figure 4. The convergence orders for the velocity doesn't always reach exactly $r+2$ due to the polynomial order r in time. Table 2 shows the number of

GMRES iterations required for convergence for these experiments. We compare the hp STMG with a pure spatial h -multigrid method. The hp STMG method exhibits superior robustness and significantly reduces the number of iterations, as the polynomial degree and mesh refinement increase. In specific settings on coarse meshes and low polynomial orders, the hp STMG can be outperformed by other strategies (e. g. pure h -multigrid, h -multigrid in space and p -multigrid in time only). However, it consistently outperforms them on finer meshes and higher polynomial degrees. Further, although polynomial coarsening $r \rightarrow r - 1$ can reduce GMRES iterations and improve p -robustness, it yields no significant gains in wall-clock time due to the slower decrease of the block size. However, the reduction of the block size through polynomial coarsening increases the efficiency significantly. In particular, halving the polynomial degree $r \rightarrow \frac{r}{2}$ provides the best improvements in solver performance.

We note that only a single smoothing step is performed on all levels. While additional smoothing steps could reduce the number of GMRES iterations and improve the h - and p -robustness, it may not improve the time to solution for matrix-free methods. We use a matrix-based smoother (4.21), so keeping the number of smoothing steps small and reducing the complexity is the most important part of the overall performance, see also [32]. In the present section, we achieve excellent h -robustness, but not full p -robustness. We revisit this topic in the following sections and address whether an increase in smoothing steps improves the p -robustness.

Table 3: Average number of GMRES iterations per subproblem \bar{n}_{iter} for different numbers of smoothing steps n_{sm} , polynomial degrees r and refinements c . We also include the number of global space-time cells (# st-cells).

c	# st-cells	$n_{\text{sm}} = 1$		$n_{\text{sm}} = 2$		$n_{\text{sm}} = 4$	
		$r = 2$	$r = 3$	$r = 2$	$r = 3$	$r = 2$	$r = 3$
4	$1.049 \cdot 10^6$	18.14	28.09	10.56	16.22	6.83	10.66
5	$1.678 \cdot 10^7$	16.97	25.72	9.32	13.79	5.83	9.17
6	$2.684 \cdot 10^8$	14.82	21.95	7.60	11.26	4.86	7.56
7	$4.295 \cdot 10^9$	12.52	18.41	6.39	9.25	3.88	6.27

Table 4: Throughput θ (5.3) for different values of n_{sm} , r and c .

c	# st-cells	$n_{\text{sm}} = 1$		$n_{\text{sm}} = 2$		$n_{\text{sm}} = 4$	
		$r = 2$	$r = 3$	$r = 2$	$r = 3$	$r = 2$	$r = 3$
4	$1.049 \cdot 10^6$	2 024 903	1 473 680	1 909 852	1 326 565	1 635 246	1 049 484
5	$1.678 \cdot 10^7$	14 312 807	11 662 467	14 217 734	11 308 509	12 540 383	8 855 231
6	$2.684 \cdot 10^8$	77 500 431	45 412 285	81 006 664	38 266 573	67 246 528	34 610 897
7	$4.295 \cdot 10^9$	181 590 442	79 615 077	157 784 452	76 728 780	148 013 169	58 091 344

5.2. Lid-driven cavity flow. We now study the more sophisticated benchmark problem of lid-driven cavity flow. The space-time mesh $\mathcal{T}_h \times \mathcal{M}_\tau$ is a uniform triangulation of the space-time domain $\Omega \times I = [0, 1]^3 \times [0, 8]$, refined globally c times. A Dirichlet profile \mathbf{v}_D is prescribed at the upper boundary $\Gamma_D = [0, 1]^2 \times \{1\} \subset \partial\Omega$ as

$$(5.2) \quad \mathbf{v}_D(x, y, z, t) = \sin\left(\frac{\pi}{4}t\right) \text{ on } \Gamma_D \times [0, 8].$$

On the other boundaries, denoted by $\Gamma_{\text{wall}} = \partial\Omega \setminus \Gamma_D$ we use no-slip boundary conditions. We employ discretizations with different polynomial degrees $r \in \{2, 3\}$ in

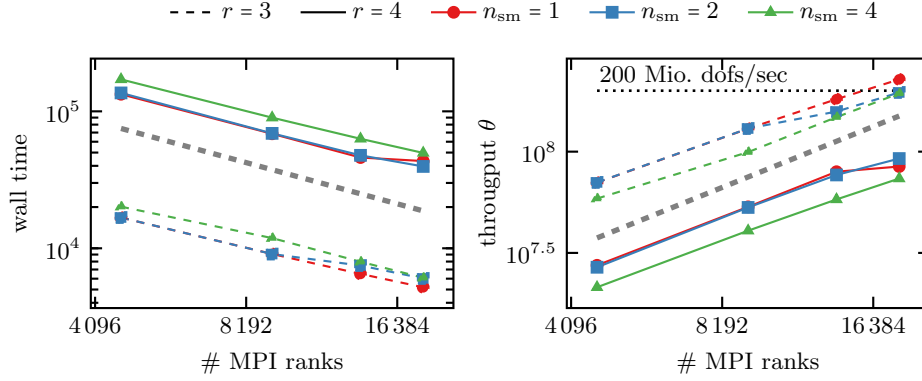


Fig. 2: Strong scaling test results for the STMG algorithm with varying numbers of smoothing steps. The left plot shows the time to solution over the number of MPI processes. The dashed gray lines indicate the optimal scaling. The right plot depicts the degrees of freedom (dofs) processed per second over the number of MPI processes.

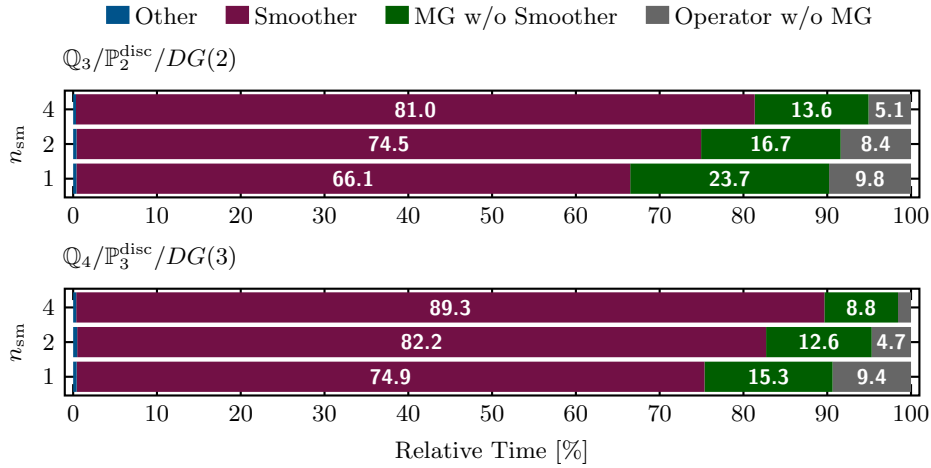


Fig. 3: Time spent in different parts of the lid-driven cavity flow simulation, executed on 18432 MPI processes. The simulations were conducted for $c = 7$, $r \in \{3, 4\}$, $n_{sm} \in \{1, 2, 4\}$.

space. For the time discretization we set $k = r$. For the strong scaling test shown in Figure 2 we set $c = 7$, which results in 2048 time cells and 2 097 152 space cells. This configuration yields 446 960 131 and 192 171 395 spatial degrees of freedom for $r = 3$ and $r = 2$, respectively, and 3 661 497 393 152 and 1 180 701 050 880 global space-time dofs. The resulting local linear systems each involve 1 787 840 524 unknowns for $r = 3$ and 576 514 185 unknowns for $r = 2$. The average number of GMRES iterations \bar{n}_{iter} for different values of $n_{sm} \in \{1, 2, 4\}$, $r \in \{2, 3\}$ and $c \in \{4, 5, 6, 7\}$ are collected in Table 3. To compare the computational efficiency, we measure the *throughput*. Let $W_{total}(n_{sm}, c, r)$ be the total walltime, and $N_{dof}(c, r)$ the total number of degrees of

freedom. The throughput $\theta(n_{\text{sm}}, c, r)$ is defined as

$$(5.3) \quad \theta(n_{\text{sm}}, c, r) = \frac{N_{\text{dof}}(c, r)}{W_{\text{total}}(n_{\text{sm}}, c, r)}.$$

In addition to the scaling test and performance of the iterative solver, we verify the convergence of our discretization by studying a goal quantity in Appendix C. In Table 4, we summarize θ using walltimes obtained on 13824 MPI ranks in the same configurations as presented in Table 3. Increasing the number of smoothing steps, n_{sm} , reduces the GMRES iterations, but the higher cost per iteration leads to increased wall times. A larger n_{sm} also improves p -robustness, which is satisfactory but could be improved. Overall, the Vanka smoother (4.21) is effective. However, cell-wise direct solves introduce significant overhead, especially at higher polynomial degrees. In Figure 3 we show the relative execution time spent in different parts of the program within the strong scaling test for different n_{sm} . The *MG w/o Smoother* segment corresponds to the hp STMG without its smoothing steps, i.e. operator evaluations and grid transfers. Its contribution decreases as the number of smoothing steps increases. In contrast, the *Smoother* segment, consistently dominates the wall time. Its cost depends on the polynomial order and continues to increase with n_{sm} . The *Operator w/o MG* part covers operator evaluations performed outside the hp STMG preconditioner, and the *Other* segment includes the time spent on source term assembly, goal quantity evaluation and tasks between time steps. The absolute time of these segments remain constant, resulting in a decrease in relative time with increasing smoothing steps.

6. Conclusions. We present an hp multigrid approach for tensor-product space-time finite element discretizing the Stokes equations. The method is highly efficient and scalable, exhibiting optimal h -robustness and satisfactory p -robustness. Even when embedded in a time-marching scheme, the proposed hp space-time multigrid method still achieves notable efficiency gains through combined space-time coarsening. The smoother is effective but expensive and represents the main computational bottleneck for higher order discretizations. Vertex-patch smoothers could further enhance p -robustness [38, 33, 43]. For these types of smoothers, replacing the direct solver with a more efficient local method becomes crucial to avoid the escalating cost at large p . The direct solves also raise concerns about memory usage. Iterative local solvers might be less resource intensive. Block-diagonal or approximate factorization approaches might preserve efficiency without incurring the cost of a full direct solver. Despite the current limitations, the method performs well and achieves throughput over 200 millions of degrees of freedom per second on problems with trillions of global degrees of freedom. It outperforms existing matrix-based implementations by orders of magnitude (cf. [4]). The proposed matrix-free hp multigrid method for tensor-product space-time finite element discretizations is efficient and scalable, making it a promising candidate for large-scale problems in fluid mechanics, fluid-structure interaction, and dynamic poroelasticity. An extension to these problems, particularly nonlinear ones (e.g. Navier-Stokes), is part of future work.

Appendix A. An Example of Multigrid Sequence Generation. We illustrate the application of Algorithm 4.3 and 4.4 by an example: Table 5 summarizes the multigrid hierarchy by listing the spatial and temporal discretization parameters for geometric and polynomial coarsening. In space, the mesh size reduces from h to $2h$ (Level 1) and $4h$ (Level 0), while the polynomial degree is reduced from 2 at Level 3 to 1 from Level 2 onward. In this example, no geometric coarsening in time is performed and polynomial coarsening in time is applied from Level 1 to Level 0.

Table 5: Multigrid Hierarchy Parameters for Each Level

Level	Space		Time		Coarsening description
	h -MG	p -MG	h -MG	p -MG	
3	h	2	τ	2	Polynomial coarsening in space
2	h	1	τ	2	Geometric coarsening in space
1	$2h$	1	τ	2	Polynomial in time, geometric in space
0	$4h$	1	τ	1	

Appendix B. Convergence plots. In Figure 4 we show the convergence in different norms for all polynomial degrees and numbers of refinement considered in Subsection 5.1. The corresponding number of iterations for each of these numerical experiments can be found in Table 2.

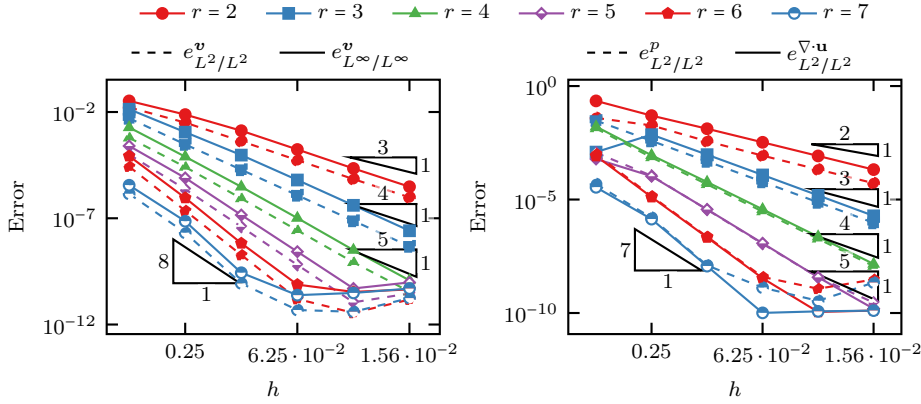


Fig. 4: Calculated errors of the velocity and pressure in various norms (velocity: L^2 , L^∞ in space-time and the L^2 -norm of the divergence in space-time, pressure: L^2 in space-time) for different polynomial orders. The expected orders of convergence, represented by the triangles, match with the experimental orders.

Appendix C. Pressure difference in lid-driven cavity flow. To assess the convergence of our discretization, we consider the normalized pressure difference

$$p_{\text{diff}}(t) = \frac{p(0.875, 0.125, 0.125, t) - p(0.875, 0.875, 0.875, t)}{p(0.875, 0.125, 0.125, t)}.$$

We normalize the pressure difference in order to better visualize the discretization error. In Figure 5 we plot $p_{\text{diff}}(t)$ over the time interval $I = [0, 8]$.

Acknowledgments. Computational resources (HPC cluster HSUper) have been provided by the project hpc.bw, funded by dtcc.bw - Digitalization and Technology Research Center of the Bundeswehr. dtcc.bw is funded by the European Union - NextGenerationEU.

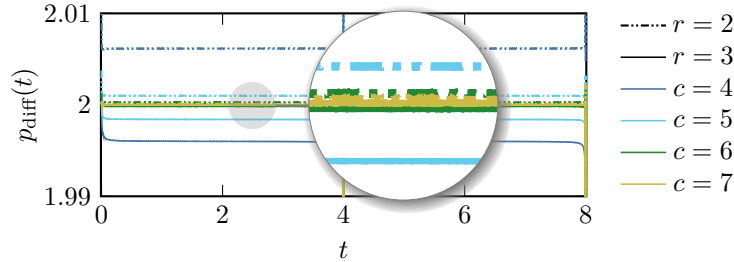


Fig. 5: Normalized Pressure difference $p_{\text{diff}}(t)$ over time.

- [1] R. ABU-LABDEH, S. MACLACHLAN, AND P. E. FARRELL, *Monolithic multigrid for implicit runge-kutta discretizations of incompressible fluid flow*, Journal of Computational Physics, 478 (2023), p. 111961, <https://doi.org/10.1016/j.jcp.2023.111961>.
- [2] P. C. AFRICA, D. ARNDT, W. BANGERTH, B. BLAIS, M. FEHLING, R. GASSMÖLLER, T. HEISTER, L. HELTAI, S. KINNEWIG, M. KRONBICHLER, M. MAIER, P. MUNCH, M. SCHRETER-FLEISCHHACKER, J. P. THIELE, B. TURCK SIN, D. WELLS, AND V. YUSHUTIN, *The deal.II library, version 9.6*, Journal of Numerical Mathematics, 32 (2024), pp. 369–380, <https://doi.org/10.1515/jnma-2024-0137>.
- [3] N. AHMED, C. BARTSCH, V. JOHN, AND U. WILBRANDT, *An assessment of some solvers for saddle point problems emerging from the incompressible Navier–Stokes equations*, Computer Methods in Applied Mechanics and Engineering, 331 (2018), pp. 492–513, <https://doi.org/10.1016/j.cma.2017.12.004>.
- [4] M. ANSELMANN AND M. BAUSE, *A geometric multigrid method for space-time finite element discretizations of the navier–stokes equations and its application to 3d flow simulation*, ACM Transactions on Mathematical Software, (2023), <https://doi.org/10.1145/3582492>.
- [5] M. ANSELMANN, M. BAUSE, N. MARGENBERG, AND P. SHAMKO, *An energy-efficient GMRES-multigrid solver for space-time finite element computation of dynamic poroelasticity*, Computational Mechanics, (2024), <https://doi.org/10.1007/s00466-024-02460-w>.
- [6] M. ANSELMANN, M. BAUSE, G. MATTHIES, AND F. SCHIEWECK, *Optimal order pressure approximation for the stokes problem by a variational method in time with post-processing*, in progress, (2025).
- [7] M. BAUSE, M. P. BRUCHHÄUSER, AND U. KÖCHER, *Flexible goal-oriented adaptivity for higher-order space-time discretizations of transport problems with coupled flow*, Computers & Mathematics with Applications, 91 (2021), pp. 17–35, <https://doi.org/10.1016/j.camwa.2020.08.028>.
- [8] M. BESIER AND R. RANNACHER, *Goal-oriented space-time adaptivity in the finite element Galerkin method for the computation of nonstationary incompressible flow*, Int. J. Numer. Math. Fluids., 70 (2012), pp. 1139–1166, <https://doi.org/10.1002/fld.2735>.
- [9] J. H. BRAMBLE, *Multigrid Methods*, Longman Scientific & Technical, Harlow, 1993.
- [10] B. CHAUDET-DUMAS, M. J. GANDER, AND A. POGOZELSKYTE, *An optimized Space-Time Multigrid algorithm for parabolic PDEs*. arXiv preprint, 2023, <https://doi.org/10.48550/arXiv.2302.13881>.
- [11] A. J. CHRISTLIEB, C. B. MACDONALD, AND B. W. ONG, *Parallel High-Order Integrators*, SIAM Journal on Scientific Computing, 32 (2010), pp. 818–835, <https://doi.org/10.1137/09075740X>.
- [12] D. CORALLO, W. DÖRFLER, AND C. WIENERS, *Space-Time Discontinuous Galerkin Methods for Weak Solutions of Hyperbolic Linear Symmetric Friedrichs Systems*, Journal of Scientific Computing, 94 (2023), p. 27, <https://doi.org/10.1007/s10915-022-02076-3>.
- [13] F. DANIELI, B. S. SOUTHWORTH, AND A. J. WATHEN, *Space-time block preconditioning for incompressible flow*, SIAM Journal on Scientific Computing, 44 (2022), pp. A337–A363, <https://doi.org/10.1137/21M1390773>, <https://epubs.siam.org/doi/10.1137/21M1390773>.
- [14] J. ERNESTI AND C. WIENERS, *Space-Time Discontinuous Petrov–Galerkin Methods for Linear Wave Equations in Heterogeneous Media*, Computational Methods in Applied Mathematics, 19 (2019), pp. 465–481, <https://doi.org/10.1515/cmam-2018-0190>.
- [15] L. FAILER AND T. RICHTER, *A parallel newton multigrid framework for monolithic fluid-structure interactions*, Journal of Scientific Computing, 82 (2021), <https://doi.org/10.1007/s10915-021-02076-3>.

- 1007/s10915-019-01113-y.
- [16] R. D. FALGOUT, S. FRIEDHOFF, T. V. KOLEV, S. P. MACLACHLAN, J. B. SCHRODER, AND S. VANDEWALLE, *Multigrid methods with space-time concurrency*, Computing and Visualization in Science, 18 (2017), pp. 123–143, <https://doi.org/10.1007/s00791-017-0283-9>.
 - [17] N. FEHN, P. MUNCH, W. A. WALL, AND M. KRONBICHLER, *Hybrid multigrid methods for high-order discontinuous Galerkin discretizations*, Journal of Computational Physics, 415 (2020), p. 109538, <https://doi.org/10.1016/j.jcp.2020.109538>.
 - [18] S. R. FRANCO, F. J. GASPAR, M. A. VILLELA PINTO, AND C. RODRIGO, *Multigrid method based on a space-time approach with standard coarsening for parabolic problems*, Applied Mathematics and Computation, 317 (2018), pp. 25–34, <https://doi.org/10.1016/j.amc.2017.08.043>.
 - [19] M. J. GANDER AND T. LUNET, *Time Parallel Time Integration*, Society for Industrial and Applied Mathematics, Philadelphia, PA, 2024, <https://doi.org/10.1137/1.9781611978025>.
 - [20] M. J. GANDER AND M. NEUMÜLLER, *Analysis of a New Space-Time Parallel Multigrid Algorithm for Parabolic Problems*, SIAM Journal on Scientific Computing, 38 (2016), pp. A2173–A2208, <https://doi.org/10.1137/15M1046605>.
 - [21] W. HACKBUSCH, *Multi-Grid Methods and Applications*, Springer, 1985.
 - [22] W. HACKBUSCH, *Parabolic multi-grid methods*, in Proc. of the Sixth Int'l. Symposium on Computing Methods in Applied Sciences and Engineering, VI, North-Holland Publishing Co., 1985, pp. 189–197.
 - [23] S. HON AND S. SERRA-CAPIZZANO, *A block Toeplitz preconditioner for all-at-once systems from linear wave equations*, ETNA - Electronic Transactions on Numerical Analysis, 58 (2023), pp. 177–195, https://doi.org/10.1553/etna_vol58s177.
 - [24] G. HORTON AND S. VANDEWALLE, *A Space-Time Multigrid Method for Parabolic Partial Differential Equations*, SIAM Journal on Scientific Computing, 16 (1995), pp. 848–864, <https://doi.org/10.1137/0916050>.
 - [25] D. JODLBAUER, U. LANGER, T. WICK, AND W. ZULEHNER, *Matrix-free monolithic multigrid methods for stokes and generalized stokes problems*, SIAM Journal on Scientific Computing, 46 (2024), pp. A1599–A1627, <https://doi.org/10.1137/22M1504184>.
 - [26] V. JOHN, *Finite Element Methods for Incompressible Flow Problems*, vol. 51 of Springer Series in Computational Mathematics, Springer, 2016, <https://doi.org/10.1007/978-3-319-45750-5>.
 - [27] N. KOHL AND U. RÜDE, *Textbook efficiency: Massively parallel matrix-free multigrid for the stokes system*, SIAM Journal on Scientific Computing, 44 (2022), pp. C124–C155, <https://doi.org/10.1137/20M1376005>.
 - [28] M. KRONBICHLER AND K. KORMANN, *A generic interface for parallel cell-based finite element operator application*, Computers & Fluids, 63 (2012), pp. 135–147, <https://doi.org/10.1016/j.compfluid.2012.04.012>.
 - [29] U. LANGER AND A. SCHAFELNER, *Adaptive space-time finite element methods for parabolic optimal control problems*, Journal of Numerical Mathematics, 30 (2022), pp. 247–266, <https://doi.org/10.1515/jnma-2021-0059>.
 - [30] U. LANGER AND A. SCHAFELNER, *Space-Time Hexahedral Finite Element Methods for Parabolic Evolution Problems*, in Domain Decomposition Methods in Science and Engineering XXVI, S. C. Brenner, E. Chung, A. Klawonn, F. Kwok, J. Xu, and J. Zou, eds., Lecture Notes in Computational Science and Engineering, Springer International Publishing, 2022, pp. 515–522, https://doi.org/10.1007/978-3-030-95025-5_55.
 - [31] U. LANGER AND O. STEINBACH, eds., *Space-Time Methods: Applications to Partial Differential Equations*, De Gruyter, 2019, <https://doi.org/10.1515/9783110548488>.
 - [32] N. MARGENBERG AND P. MUNCH, *A Space-Time Multigrid Method for Space-Time Finite Element Discretizations of Parabolic and Hyperbolic PDEs*. arXiv preprint, 2024, <https://doi.org/10.48550/arXiv.2408.04372>.
 - [33] A. MIRAČI, J. PAPEŽ, AND M. VOHRALÍK, *A Multilevel Algebraic Error Estimator and the Corresponding Iterative Solver with p-Robust Behavior*, SIAM Journal on Numerical Analysis, 58 (2020), pp. 2856–2884, <https://doi.org/10.1137/19M1275929>.
 - [34] P. MUNCH, I. DRAVINS, M. KRONBICHLER, AND M. NEYTCHEVA, *Stage-Parallel Fully Implicit Runge–Kutta Implementations with Optimal Multilevel Preconditioners at the Scaling Limit*, SIAM Journal on Scientific Computing, (2023), pp. S71–S96, <https://doi.org/10.1137/22M1503270>.
 - [35] P. MUNCH, T. HEISTER, L. PRIETO SAAVEDRA, AND M. KRONBICHLER, *Efficient Distributed Matrix-free Multigrid Methods on Locally Refined Meshes for FEM Computations*, ACM Transactions on Parallel Computing, 10 (2023), pp. 3:1–3:38, <https://doi.org/10.1145/3580314>.

- [36] R. H. NOCHETTO, S. A. SAUTER, AND C. WIENERS, *Space-time Methods for Time-dependent Partial Differential Equations*, Oberwolfach Reports, 14 (2018), pp. 863–947, <https://doi.org/10.4171/owr/2017/15>.
- [37] M. OLSHANSKII, *Multigrid analysis for the time dependent stokes problem*, Mathematics of Computation, 81 (2012), pp. 57–79, <https://doi.org/10.1090/S0025-5718-2011-02494-4>, <https://www.ams.org/mcom/2012-81-277/S0025-5718-2011-02494-4/>.
- [38] L. F. PAVARINO, *Additive Schwarz methods for thep-version finite element method*, Numerische Mathematik, 66 (1993), pp. 493–515, <https://doi.org/10.1007/BF01385709>.
- [39] W. PAZNER AND P.-O. PERSSON, *Stage-parallel fully implicit Runge–Kutta solvers for discontinuous Galerkin fluid simulations*, Journal of Computational Physics, 335 (2017), pp. 700–717, <https://doi.org/10.1016/j.jcp.2017.01.050>.
- [40] R. PICARD AND D. MCGHEE, *Partial Differential Equations: A unified Hilbert Space Approach*, De Gruyter, 2011, <https://doi.org/10.1515/9783110250275>.
- [41] L. PRIETO SAAVEDRA, P. MUNCH, AND B. BLAIS, *A Matrix-Free Stabilized Solver for the Incompressible Navier-Stokes Equations*, 2024, <https://doi.org/10.2139/ssrn.4981567>.
- [42] J. ROTH, J. P. THIELE, U. KÖCHER, AND T. WICK, *Tensor-Product Space-Time Goal-Oriented Error Control and Adaptivity With Partition-of-Unity Dual-Weighted Residuals for Nonstationary Flow Problems*, Computational Methods in Applied Mathematics, (2023), <https://doi.org/10.1515/cmam-2022-0200>.
- [43] J. SCHÖBERL, J. M. MELENK, C. PECHSTEIN, AND S. ZAGLMAYR, *Additive Schwarz preconditioning for p-version triangular and tetrahedral finite elements*, IMA Journal of Numerical Analysis, 28 (2008), pp. 1–24, <https://doi.org/10.1093/imanum/dri046>.
- [44] B. S. SOUTHWORTH, O. KRZYSIK, W. PAZNER, AND H. D. STERCK, *Fast solution of fully implicit runge–kutta and discontinuous galerkin in time for numerical PDEs, part i: the linear setting*, SIAM Journal on Scientific Computing, 44 (2022), pp. A416–A443, <https://doi.org/10.1137/21M1389742>, <https://epubs.siam.org/doi/abs/10.1137/21M1389742>.
- [45] O. STEINBACH, *Space-Time Finite Element Methods for Parabolic Problems*, Computational Methods in Applied Mathematics, 15 (2015), pp. 551–566, <https://doi.org/10.1515/cmam-2015-0026>.
- [46] O. STEINBACH AND H. YANG, *An Algebraic Multigrid Method for an Adaptive Space–Time Finite Element Discretization*, in Large-Scale Scientific Computing, I. Lirkov and S. Margenov, eds., Lecture Notes in Computer Science, Springer International Publishing, 2018, pp. 66–73, https://doi.org/10.1007/978-3-319-73441-5_6.
- [47] P. S. VASSILEVSKI, *Multilevel Block Factorization Preconditioners: Matrix-based Analysis and Algorithms for Solving Finite Element Equations*, Springer, 2008.
- [48] A. VORONIN, G. HARPER, S. MACLACHLAN, L. N. OLSON, AND R. S. TUMINARO, *Monolithic Multigrid Preconditioners for High-Order Discretizations of Stokes Equations*. arXiv preprint, 2024, <https://doi.org/10.48550/arXiv.2407.07253>.
- [49] C. WIENERS, *A space-time discontinuous Galerkin discretization for the linear transport equation*, Computers & Mathematics with Applications, 152 (2023), pp. 294–307, <https://doi.org/10.1016/j.camwa.2023.10.031>.
- [50] H. WOBKER AND S. TUREK, *Numerical Studies of Vanka-Type Smoothers in Computational Solid Mechanics*, Adv. Appl. Math. Mech., (2009).